COMITATO NAZIONALE PER L'ENERGIA NUCLEARE
Laboratori Nazionali di Frascati

LNF-71/91
20 Dicembre 1971

B. Bartoli, F. Felicetti, G. Marini, A. Nigro, H. Ogren, V. Silvestrini and F. Vanoli: ELECTRON-POSITRON INTERACTIONS AT HIGH ENERGIES. -

Servizio Documentazione
dei Laboratori Nazionali di Frascati del CNEN
Casella Postale 70 - Frascati (Roma)

Laboratori Nazionali di Frascati del CNEN
Servizio Documentazione

LNF-71/91
20 Dicembre 1971

B. Bartoli, F. Felicetti, G. Marini(x), A. Nigro(o), H. Ogren, V. Silvestrini and F. Vanoli(o): ELECTRON-POSITRON INTERACTIONS AT HIGH ENERGIES. -

(Submitted to the Physical Review).

ABSTRACT. -

We present the results of an experiment performed at Adone, the Frascati 2×1.5 GeV e^+e^- storage ring. During ~ 1500 hours of running time, we have collected a total of 5164 electron-positron elastic scattering events (integrated luminosity $\mathcal{L} = 3.5 \times 10^{35}$ cm^{-2}) and 605 non-coplanar events of the type $e^+e^- \rightarrow a^{\pm} + b^{\pm}$ + anything (effective integrated luminosity $\mathcal{L} = 2.5 \times 10^{35}$ cm^{-2}), at C.M. energies ranging from 1.4 to 2.4 GeV.

The yield of the elastic scattering events is in good agreement with the predictions of quantum electrodynamics: $R = \sigma_{exp} / \sigma_{QED} = 1.05 \pm 0.04$ ($\pm 6.5\%$ systematic).

The non-coplanar events appear to be of hadronic nature, and are produced with a total cross-section as large as 50 - 90 nbarns. The evaluation of the cross-sections for some channels ($e^+e^- \rightarrow \pi^+\pi^-\pi^+\pi^-$; $e^+e^- \rightarrow \pi^+\pi^-\pi^+\pi^-$ + neutrals; $e^+e^- \rightarrow 3\pi^+3\pi^-$) contributing to these multihadron processes is also given.

I. - INTRODUCTION. -

We present here the final results of an experiment performed during the 1970-71 at Adone, the Frascati 2×1.5 GeV e^+e^- storage ring. The experiment was originally designed mainly to search for possible enhancements in the yield of particles produced in e^+e^- interactions as a function of the total C.M. energy in the range of energies between 1.4 and 3.0 GeV, which could indicate the existence of new vector bosons. Events due to e^+e^- wide angle elastic scattering (Bhabha events) were collected at the same time, both as a test of

---

(x) - Istituto di Fisica dell'Università di Roma e Sezione di Roma dell'INFN, Roma (Italy).
(o) - Istituto di Fisica dell'Università di Napoli e Sezione di Napoli dell'INFN, Napoli (Italy).

quantum electrodynamics (QED) in the region of space-like momentum transfers to the virtual photon up to 2.5 $(GeV/c)^2$ and as a monitor reaction for the hadronic channels.

When Adone came into operation, the electron positron annihilation into hadrons, through the vector mesons ϱ, ω, φ, had already been extensively studied at Orsay[1] and Novosibirsk[2]. As a crude extension of ϱ, ω, φ dominance model up to 2 GeV or more, the most popular tendency was to expect the production of hadrons to be very depressed at those relatively high energies.

It is now well known (see the preliminary results of this experiment published in 1970[3] and 1971[4] and confirmed by the results from other groups[5,6]) that the cross section for production of many hadrons in e^+e^- interactions turns out to be surprisingly larger than one would have expected.

These results have stimulated considerable theoretical activity[7]. Among the most attractive theories are the so called "point-like" models trying to relate these large values of the cross sections to the analogous well known results on the space-like channel obtained by the SLAC-MIT collaboration[8] studying the deep inelastic scattering of electron on protons. The problem of their interpretation is still quite open and much more work must be done both experimentally and theoretically in this field.

Concerning the results we are presenting in this paper, we would like to make a final remark. We are aware that even in this final version some features of our results are to a certain degree qualitative. In fact our apparatus (as well as all the other "first generation" apparata operating at Adone) had not been designed in order to study the phenomenon which turned out to be the most important at the Adone energies, namely the production of high multiplicity final states. Nevertheless we have thought it important to push the phenomenological interpretation as far as possible for two reasons, namely: i) to give the maximum possible information for the design of new experimental apparata; ii) because the orders of magnitude obtained for the cross sections are so large that they open by themselves a new problematic in the study of the structure of the hadrons and of their electromagnetic current.

II. - THE EXPERIMENTAL APPARATUS. -

The experimental apparatus, shown in Fig. 1, surrounds one of the straight sections of Adone and covers about 0.35 of the total solid angle as seen from the center of the apparatus[9].

Each of the four identical telescopes T_i consists of:

a) four plastic scintillation counters A_i, B_i, C_i, D_i;
b) two magnetostrictive monogap wire spark chambers SC α_i, SC β_i, which measure φ, the azimuthal direction of the final state particles (z-axis along the beam direction);
c) the following absorbers: 1.3 cm Al between A_i and B_i; 0.7 cm Pb between B_i and C_i and between C_i and D_i. Signal pulses from the lead-scintillator-sandwich counter (C_i+D_i) were used for pulse height analysis to discriminate showering electrons from minimum ionizing particles.

These telescopes T_i cover the following angles, as measured from a coordinate system centered on the apparatus (z, along the e^+e^- direction; x, toward the center of the Adone ring):

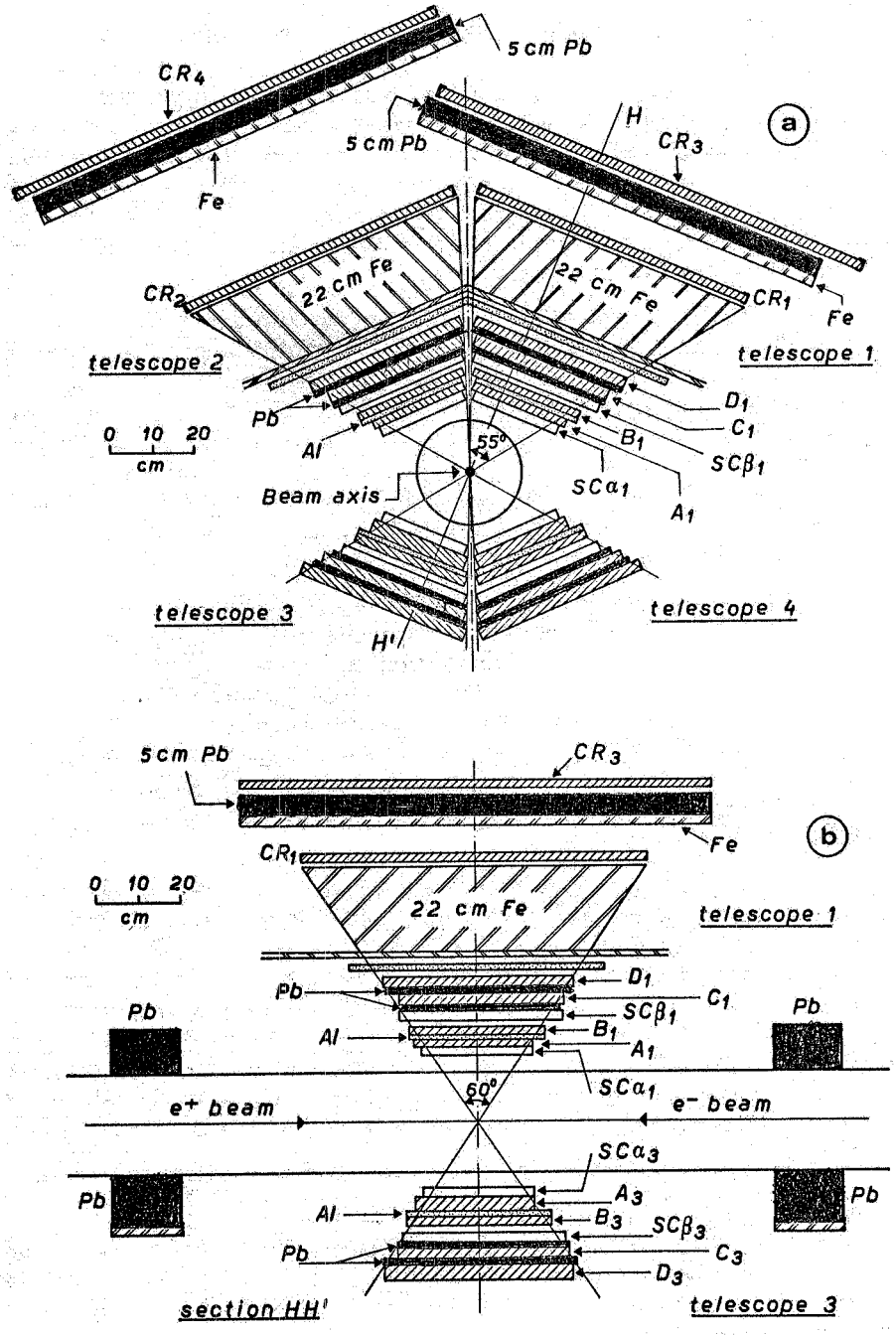

FIG. 1 - The experimental apparatus. a) Section orthogonal to the beam axis: A_i, B_i, C_i, D_i are plastic scintillator counters; Sc α_i and Sc β_i are magnetostrictive monogap wire chambers; CR_i's are veto counters against cosmic rays; b) Section (along H,H') in a plane through the beam direction and orthogonal to a pair of opposite telescopes.

T_1 ($60^o < \theta < 120^o$, $28^o < \varphi < 83^o$) T_2 ($60^o < \theta < 120^o$, $97^o < \varphi < 152^o$)

T_3 ($60^o < \theta < 120^o$, $208^o < \varphi < 263^o$) T_4 ($60^o < \theta < 120^o$, $277^o < \varphi < 332^o$)

A thick absorber (22 cm Fe) and a roof of veto counters CR_1 and CR_2 above the apparatus reduce the detected cosmic ray flux by a factor $\gtrsim 100$. On the other hand the emitted particles we are interested in have only a relatively small probability of emerging from the Fe and thus triggering the anticoincidence counters CR_1, CR_2: for the electrons this is due to the absorption of their electromagnetic shower, while for the hadrons this results from being stopped or nuclearly absorbed.

In a second set of measurements we have added a second roof, consisting of 1.5 cm of Fe and 5 cm of Pb, and two additional counters CR_3 and CR_4 (see Fig. 1). During this second set of measurements, CR_3 and CR_4 were used in anticoincidence, while CR_1, CR_2 were simply recorded in association with each event. From the number of the detected "marked" events (i.e. the events not vetoed by $CR_3 + CR_4$ but in which CR_1 or/and CR_2 were triggered) we where able to measure the anticoincidence corrections to be applied to the first set of data (i.e. with $CR_1 + CR_2$ in AC) and obtain as well direct information on the penetration of the detected particles.

A charged particle in telescope T_i is defined by the coincidence $\tau_i \equiv A_i B_i (C_i + D_i)$. A neutral particle is then defined as $\mathcal{N}_i \equiv (\bar{A}_i + \bar{B}_i)(C_i + D_i)$. Any coincidence of two or more charged particles (τ_i), each in a different telescope, defines the "master" coincidence, the CR counters being set in anticoincidence. ($CR = CR_1 + CR_2$ in the first set of measurements, while $CR = CR_3 + CR_4$ in the second set). To give a τ_i coincidence a particle must thus traverse 24 g/cm^2 of absorber, corresponding to $\sim 1.9\ X_o$ radiation lengths; to reach CR_1, CR_2 it must traverse $15\ X_o = 203$ g/cm^2; to be vetoed by CR_3, CR_4 it must traverse $25.2\ X_o = 282$ g/cm^2.

Consequently, if the particle is a pion, it must have a minimum kinetic energy of ~ 75 MeV to be detected (i.e. to give a τ_i coincidence). To be marked (or vetoed) by $CR_1 + CR_2$ the pion must have $\gtrsim 350$ MeV, while pions with more than ~ 500 MeV are vetoed by CR_3 and CR_4 unless they are absorbed by nuclear interaction (actually the fraction of particles absorbed is quite large: e.g. 85% of 400 MeV pions). On the other hand practically all the electrons with less than 1.2 GeV are absorbed before being vetoed by CR_3, CR_4, while the fraction of the electrons able to trigger $CR_1 + CR_2$ strongly depends on the energy, increasing from zero at $E \lesssim 500$ MeV up to $\sim 15\%$ at 1.2 GeV (see next section IV.3).

When a master trigger occurs a PDP8 computer records:

i) which coincidences τ_i (or $\mathcal{N}_i$) were involved in the event;
ii) the azimuthal coordinates (i.e. orthogonal to the beam direction) of the sparks in all the chambers SC α_i, SC β_i (with the restriction that when there is more than one track in the same chamber, only the closest one to the magnetostrictive pick up is detected[10]);
iii) the pulse height H_i in the lead-scintillator sandwich $(C_i + D_i)$ for each telescope T_i;
iv) the time separation Δt between the occurence of the event and a timing signal fixed to the zero crossing of the radio frequency (RF) accelerating voltage of the storage ring[11].

All this information is recorded, event by event, on a magnetic tape for a later analysis on the 1108 Univac computer of the University of Rome.

During the running of the experiment, auxiliary information was accumulated with the PDP8 in a live display (e.g. histograms of uncorrelated pulse height spectra from C_i+D_i for each telescope; the time distribution of the collected events; the distribution of the sparks in the various chambers, etc.) thus allowing a continuous check of the performance of the whole experimental apparatus.

III. - DATA COLLECTION AND INITIAL REDUCTION. -

The results we present here have been collected between January-April 1970 and between September 1970 - February 1971.

The effective total running time was ~1500 hours corresponding to a total integrated luminosity of the machine $\mathcal{L} = \int L\,dt = 3.5\ 10^{35}\ cm^{-2}$(12). The runs were performed at several values of the C.M. energy $E_+ + E_-$ ranging from 1.4 GeV to 2.4 GeV.

In Tab. I are listed, for each C.M. energy, the running time and the corresponding raw integrated luminosity. We have also marked with a star the measurements in which counters CR_3+CR_4 were set in anticoincidence (2nd set of measurements, see section II). The other runs were instead performed with CR_1+CR_2 in anticoincidence (1st set, see section II).

The quoted luminosities were evaluated by measuring with a "monitor" apparatus the yield of events from a process of known cross section, namely e^+-e^- scattering at small angles. This Bhabha scattering "monitor" apparatus(13), consisting of two symmetrical telescopes covering a range of C.M. angles, θ, between 3.5° and 6° (corresponding to four-momentum transfer to the virtual photon less than ~100 MeV/c), was operated by the "$\mu\pi$ group" (see ref. (5)) in a contiguous straight section of Adone. The overall uncertainty in the absolute normalization of the monitor is estimated to be $\pm 5\%$. In addition by analyzing the relative variations of counting rates in the two simmetric telescopes we have evaluated as $\pm 7\%$ an additional time dependent uncertainty mainly due to erratic changes in the position of the beams with respect to the monitor apparatus(14).

Over the total running period of this experiment we have collected a total of ~10^6 trigger events. The reasons for this high counting rate are the following. First, we have operated the master coincidence (between the telescopes T_i) with a very large resolving time τ ($\tau \cong 40$ nsec). This allows us, on the basis of the analysis of the Δt distribution of the events, to very accurately define a posteriori the time interval in which the two bunches of e^+ and e^- collide, and also provides a very powerfull way to evaluate the cosmic ray (C.R.) contamination to the data. In fact (see Fig. 2(a)) a typical Δt distribution, as it comes out from the computer, shows a very clear peak ($\sim$ 2nsec h.w.h.m.) corresponding to the beam-beam impact, superimposed on a smooth background due to cosmic rays. Using these distributions we can define an interval of Δt for events in-time with the beam-beam interaction.

Secondly, the pulse height thresholds of the discriminators were set much lower than the value corresponding to minimum ionizing particles. Although this introduces in the trigger rates a great amount of machine background, it permits a posteriori a much more reliable separation of the minimum ionizing

particles from the background, taking into account any long period drifts in the pulse height spectrum. As an example, in Fig. 2(b) a typical plot of H_1 vs H_3 for the collected events is shown. A cluster corresponding to minimum ionizing particles (mainly cosmic rays) is clearly visible and quite well separated from the low pulse height background. We can thus define, for each telescope T_i, two values, $H_{i,min}$ and $H_{i,max}$, within which all the minimum ionizing particles are confined.

The first steps of the analysis thus consist in selecting, run by run and energy by energy, all the events which occur in time with the beam-beam impact (in time events) excluding in this way the majority of the C.R. events (out-of-time events); and in rejecting the low pulse height machine background events, by appropriately selecting the values for each telescope of the low pulse height cut $H_{i,min}$.

The selection of the events we are interested in and the identification of the particles, is made by observing the time occurrence of the event, the particle pulse heights and the coplanarity angle between the tracks in different te-

TABLE I

Running times and integrated luminosities. The rows marked with a star refer to runs in which counters CR_3+CR_4 were set in anticoincidence with the trigger (2nd set of measurements, see Section II).

C.M. energy $E_+ + E_-$ (GeV) (1)	Running time (hours) (2)	Integrated luminosity $\mathcal{L}$ (cm^{-2}) (3)
1.40	85	68×10^{32}
1.40*	135	113
1.50	45	52
1.50*	163	280
1.60	62	77
1.65	77	114
1.70	84	126
1.75	96	135
1.80	76	135
1.85	119	260
1.85*	87	420
1.90	58	134
2.00	119	290
2.40	78	148
2.40*	221	1147
Totals	1505	3499×10^{32}

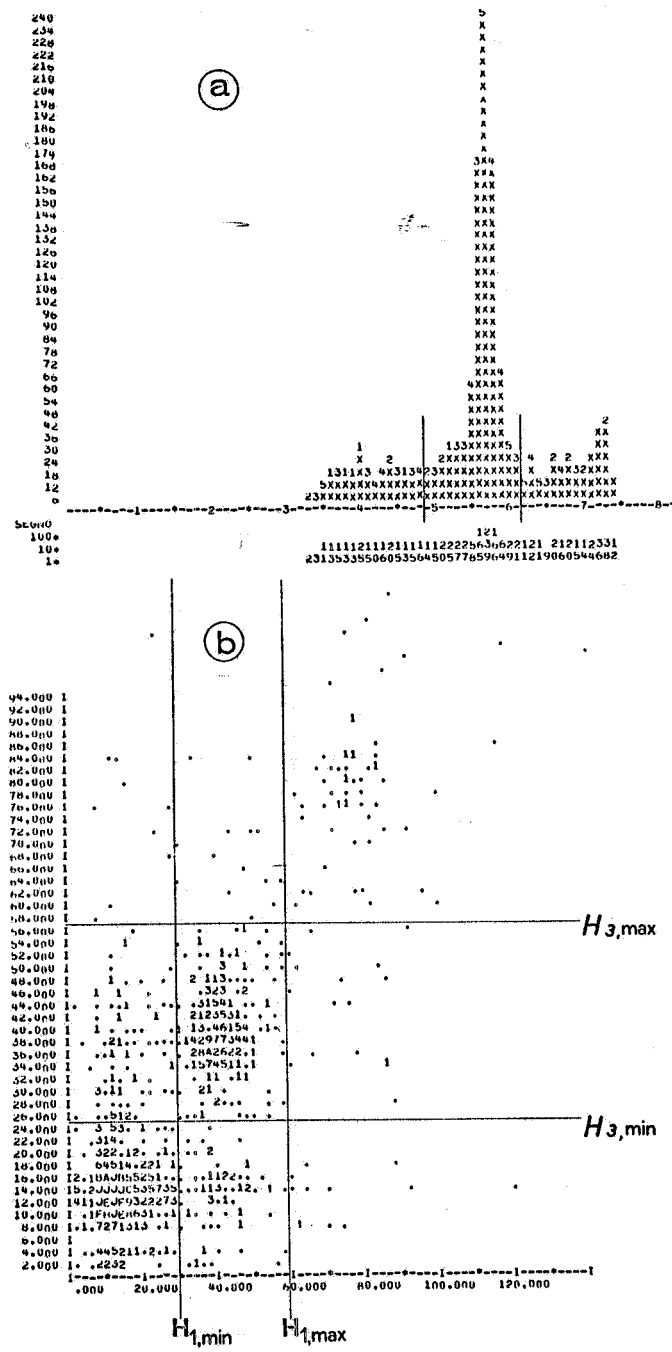

FIG. 2 - Typical computer outputs for preliminary analysis. a) Δt distribution of unselected events (Δt is the time separation between the occurrence of the event and a reference time fixed with the zero crossing of the RF accelerating voltage of the storage ring). b) Pulse height plot H_3 vs H_1 for $(\tau_1 \cdot \tau_3)$ unselected events.

lescopes. In the next section we will discuss those events determined to be e^+e^- wide angle elastic scattering. In section V, the multibody hadron events will be discussed.

IV. - REACTION $e^+e^- \rightarrow e^+e^-$. -

IV.1. - Selection of the events. -

The e^+e^- elastic scattering events are to be selected among the events which give a coincidence between opposite telescopes $(T_1 \cdot T_3)$ and $(T_2 \cdot T_4)$, and which occur in-time with the beam-beam interaction. As will be shown in this section, such a selection is possible in our apparatus simply on the basis of the pulse height analysis in the sandwich counter $(C_i + D_i)$, without the use of our experimental information on the geometry of each event.

Let us first examine the pulse height distributions. Fig. 3(a) shows a typical pulse height plot of H_1 vs H_3 for $(T_1 \cdot T_3)$ events which are in-time with the beam-beam impact. Two heavy populated region are visible in the plot. The low pulse height region, confined between $H_{i,\,min}$ and $H_{i,\,max}$, contains the minimum ionizing particle (mostly cosmic rays). The large pulse height region $(H_i \geq H_{i,\,max},\ i = 1, 3)$ contains events with both the detected particle producing a detectable shower. We designate this large pulse height region as the [e, e] region. The in-time events in this [e, e] region ([e, e] events) are good candidates to be $e^+e^- \rightarrow e^+e^-$ scattering events. The plot for out-of-time events, which turn out to be cosmic rays, shows only the cluster corresponding to minimum ionizing particles while the [e, e] region appears practically empty (see Fig. 3(b)). This shows that the [e, e] in-time events have only a small contamination from cosmic rays.

Further the other information we have from track reconstruction using the wire spark chambers, allows us to conclude that all but a small fraction of the [e, e] in-time events are e^+e^- elastic scattering events.

The track analysis of in-time [e, e] events is shown in Figs. 4(a), (b), (c). Fig. 4(a) shows the non-coplanarity angle $\Delta\varphi$ distribution, where $\Delta\varphi$ is the angle between the two planes which contain each of the two tracks and are parallel to the beam axis[15]. The [e, e] events clearly appear to be coplanar (i. e. $\Delta\varphi \simeq 0$), the $\pm 3^\circ$ angular spread (h.w.h.m.) being due to spark chamber resolution and multiple scattering in the vacuum chamber walls ($1.2\ g/cm^2 = 0.0083\ X_o$ of Fe) and in the telescope absorbers ($12.8\ g/cm^2 = 0.46\ X_o$). In Fig. 4(b) for the particles constituting the in-time [e, e] events a histogram is displayed of the distance, L, between their tracks and the axis of the beam. L is positive or negative according to the relative position of the particle trajectory with respect to the beam line. From this figure (in which all the four telescopes have been added) almost all the events appear to originate within $\pm$ 5 mm (h. w. h. m.) of the beam region. Also in this case multiple scattering and spark chamber resolution account for the observed width (the transverse dimensions of the beam are actually $\simeq (1 \times 1)\ mm^2$). This interpretation of the experimental widths of $\Delta\varphi$ and L distributions is confirmed in Fig. 4(c). In fact the clear correlation observed between $\Delta\varphi$ and the average distance, $\bar{L}$, of the two tracks from the beam, is what one could expect if all of the events originate with $\Delta\varphi = 0$ in the $(1 \times 1)\ mm^2$ source region, and the outcoming particles are scattered before crossing the spark chambers. Finally from the Δt distribution of all the [e, e] events, shown in Figure 4 (d), we can precisely define the interval of time in which the impact of the

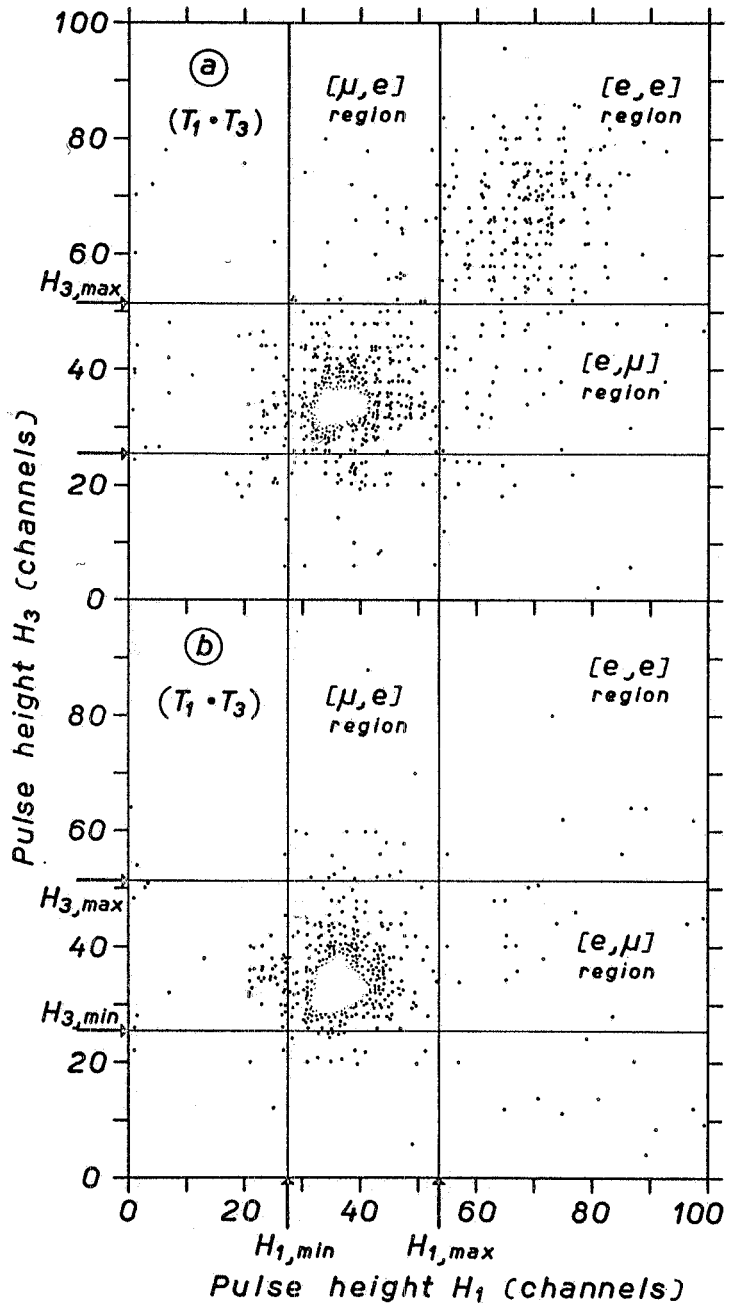

FIG. 3 - Plot of pulse heights for $(T_1 \cdot T_3)$ events. a) Events in-time with the beam-beam impact; b) Out-of-time events.

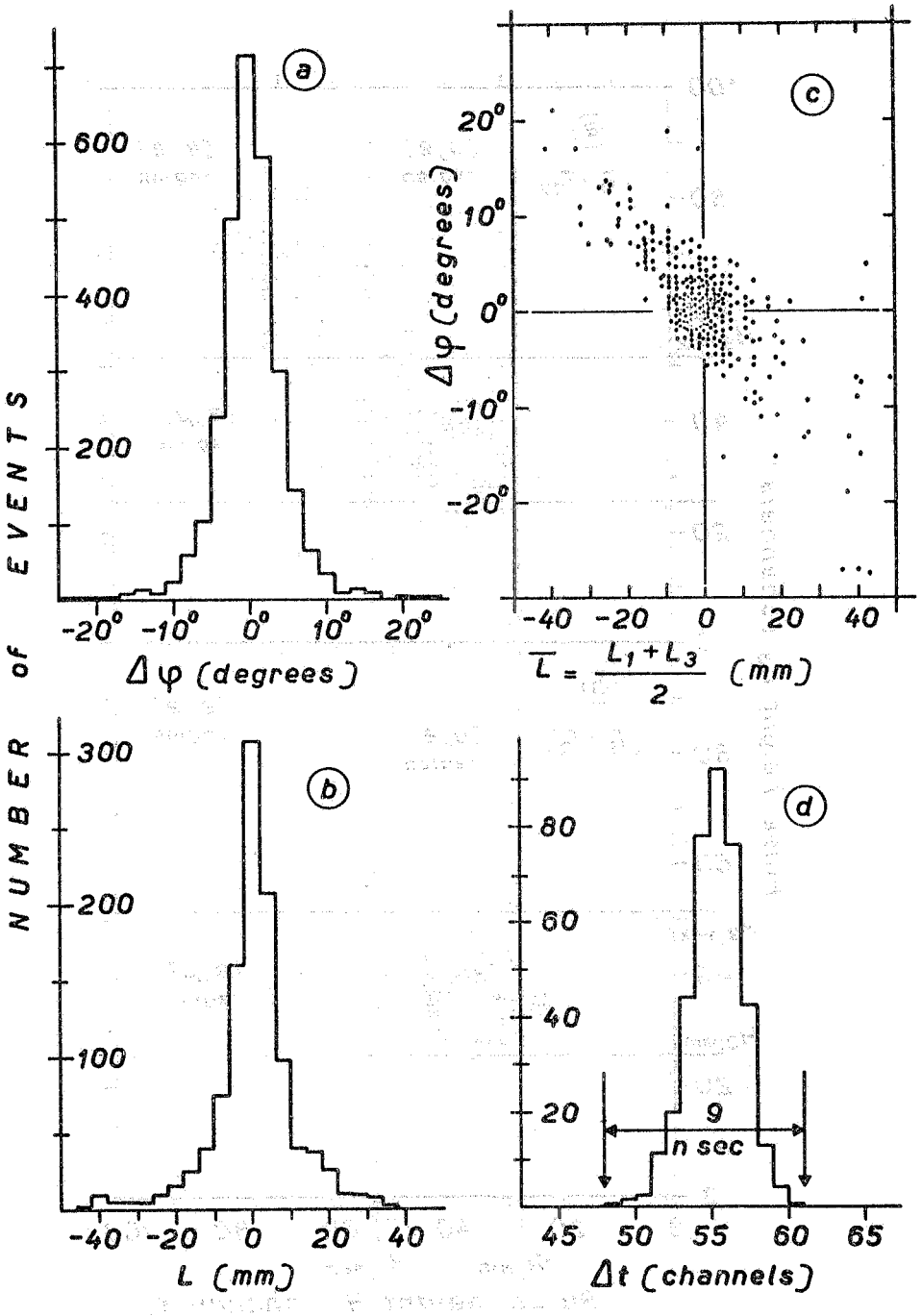

FIG. 4 - Track and time analysis of a sample of [e, e] events. a) $\Delta\varphi$ distribution for in-time events; b) L distribution for in-time events; c) $\Delta\varphi$ versus $\bar{L}$ plot for in-time events; d) Δt distribution for all the [e, e] events coming from the source region.

two bunches of e^+ and e^- occurs. The collision peak is as narrow as 3 nsec (f.w.h.m.) and the fraction of events outside of the in-time interval (9 nsec wide) is absolutely negligible.

From the previous considerations we can conclude that (apart from small background subtractions discussed later, see section IV.2) the [e, e] events are two body events, with charged, showering particles originating in e^+e^- collisions: thus they are e^+e^- elastic scattering events.

A reliable track analysis of the data requires that all four chambers involved in the event have correctly fired. Since the efficiency of our monogap spark chambers has been measured to be about ~ 0.85[16] there is a sizeble fraction ($\sim 50\%$) of [e, e] events which do not have all four chambers firing. However, we have concluded from the above track analysis of the "4-chamber"electron events (i.e. [e, e] events in which all four chambers have fired) that practically all the [e, e] in-time events that satisfy the mentioned pulse height requirements, are e^+e^- elastic scattering events. So for the evaluation of the Bhabha cross section we can use all the detected [e, e] events irrespective of spark chamber information. In this way, we have considerably higher statistics (while the background subtractions remain still quite small, see next section IV.2) and more importantly we avoid any problem connected with the spark chamber inefficiencies.

During 1505 hours of running time, with an integrated luminosity $\mathcal{L} \simeq$ $\simeq 3.5 \times 10^{35}$ cm^{-2}, we have collected a total of 5164 [e, e] events in the C.M. energy range 1.4 - 2.4 GeV. They are listed at each C.M., $E_+ + E_-$, in column (3) of Table II.

IV.2. - Background subtractions. -

There are two different types of background subtractions:

a) cosmic rays background which can be easily experimentally determined from the number of out-of-time [e, e] events (appropriately normalized according to the ratio of the widths of the "out-of-time" and "in-time" intervals). This subtraction is of the order of $\sim 2\%$ (see column (4) Table II);

b) a contamination due to interactions of either beam with the residual gas in the storage ring. For the purpose of evaluating this contamination we have performed "background" runs with only a single beam or with two separated beams stored in the ring. In these "background" runs during ~ 600 hours we have collected a total of ~ 64 [e, e] events occurring in the in-time interval. In order to correctly subtract the contamination from electron-gas interactions from our data we must deduce the appropriate normalization factor to be applied to these background events. The value of this normalization factor was obtained by monitoring the rate of each single telescope T_i during both the "background" and the colliding beam runs. The single telescope rates $\dot{\tau}_i$'s, after correction for cosmic rays, are proportional to the product of the beam currents and the residual gas density in the machine. This fact has been checked by intercalibration measurements of the single telescope rates and the single beam-gas bremsstrahlung rate $\dot{B}$: the ratio $\dot{\tau}_i/\dot{B}$ was found to be constant to within $\sim 1\%$ as a function of the beam intensity and gas pressure, over the working range of this experiment. The normalization factor (which is the same regardless of which telescope T_i is used as a basis for the normalization) varies, of course, for each experimental run depending on the relative

TABLE II

e^+e^- elastic scattering results. The rows marked with a star refer to runs in which the counters CR_3, CR_4 were set in anticoincidence with the trigger. (2nd set of measurements, see Section II). Quoted errors are only statistical.

C.M. energy $E_+ + E_-$ (GeV) (1)	integrated luminosity (cm^{-2}) (2)	collected [e, e] events (3)	normalized C.R. background (4)	normalized beam-gas background (5)	corrected e^+e^- Bhabha events (6)	m small-angle monitor events (7)	$R_{exp} = \frac{\sigma(e^+e^- \to e^+e^-)}{\sigma_{theory}}$ (8)	$\langle q^2 \rangle$ $(GeV/c)^2$ (9)
1.4	68×10^{32}	212	3.9±1.2	0.2± 0.7	803±47	198.4×10^3	.967±.056	0.87
1.4*	113×10^{32}	306	5.3±1.2	-0.6± 0.9				
1.5	52×10^{32}	141	3.6±1.1	0.2± 0.8	1158±47	308.9×10^3	1.011±.043	0.95
1.5*	280×10^{32}	738	13.6±1.9	-1.6± 2.4				
1.6	77×10^{32}	176	4.5±1.2	1.1± 1.2	234±22	64.6×10^3	1.055±.098	1.08
1.65	114×10^{32}	187	3.8±1.1	2.1± 1.8	242±21	87.6×10^3	.829±.073	1.14
1.7	126×10^{32}	259	3.8±1.1	3.2± 2.2	350±26	89.8×10^3	1.197±.091	1.21
1.75	135×10^{32}	192	4.2±1.2	3.7± 2.3	251±23	88.3×10^3	.894±.083	1.29
1.8	135×10^{32}	226	3.1±1.0	4.8± 2.6	299±25	81.3×10^3	1.164±.097	1.36
1.85	260×10^{32}	417	7.7±1.6	2.6± 2.3	1551±59	377.4×10^3	1.312±.048	1.44
1.85*	420×10^{32}	825	7.2±1.5	5.6±10.0				
1.9	134×10^{32}	186	4.2±1.2	8.6± 3.2	231±21	68.3×10^3	1.126±.105	1.52
2.0	290×10^{32}	328	7.6±1.6	30.2± 6.0	389±31	128.2×10^3	1.025±.082	1.68
2.4	148×10^{32}	102	3.6±1.1	4.0± 2.7	1102±55	302.2×10^3	1.228±.060	2.42
2.4*	1147×10^{32}	869	15.1±2.1	69.5±17.9				
Totals	3499×10^{32}	5164	91.2±5.3	133.6±22.5	6610±123	1795.9×10^3		

running times and the C.M. energies. The beam-gas contamination is near zero at low energy, but rises to $\sim 8\%$ at 2.4 GeV C.M. energy. The average contamination for the full sample of $[e, e]$ is $\sim 2\%$ (see column (5) Table II).

After background subtractions are performed, we are left with a total of 4939 $[e, e]$ elastic scattering events.

IV.3. - Corrections to the data. -

Several small corrections must be applied to the above background subtracted $[e, e]$ events:

a) "Shower correction". - Since the probability that an electron will produce a detectable shower in the sandwich counter (C_i+D_i) is not 100%, we expect that a small fraction of events $e^+e^- \to e^+e^-$ will not appear in the $[e, e]$ region of Fig. 3. To evaluate the size of this "shower correction" we have analized the events which fall in the $[\mu, e]$ regions of Fig. 3 (i.e. the events in which only one particle gives rise to a shower with a pulse height larger than $H_{i,\,max}$). We find that their L and $\Delta\varphi$ distributions (see Fig. 5(a) and (b)) are the same as for the $[e, e]$ events as we expect if these in-time $[\mu, e]$ events are true e^+e^- scattering events. The only difference is the presence in the $\Delta\varphi$ distribution of a long tail toward the large $\Delta\varphi$ values (see Fig. 5(c)) due to the occurrence of hadronic non-coplanar events we will discuss in more detail in the next section V.2. After appropriate background subtractions are performed, from the number of $[\mu, e]$ events we are able to determine the probability, ε_μ, for an electron to have a pulse height less than $H_{i,\,max}$. (In fact the probability for an event to appear in a $[\mu, e]$ region is $\varepsilon_\mu(1-\varepsilon_\mu)$). This has been done at each C.M. energy, since the value of ε_μ clearly depends on the energy of the electron: we found experimentally that it ranges from $\varepsilon_\mu = 4,6\%$ at 2.4 GeV C.M. energy up to $\varepsilon_\mu = 12.6\%$ at 1.4 GeV. The experimental values of ε_μ and the corresponding correction factors $F_S = (1-\varepsilon_\mu)^{-2}$ to be applied for this effect to the $[e, e]$ events, are listed in columns (2) and (3) of Table III at each C.M. energy $E_+ + E_-$.

b) "CR veto correction". - In the first set of measurements (see section II, and Table I and II) an e^+e^- event is lost if one of the electrons passes through the 22 cm of Iron absorber and produces an anticoincidence pulse in counters CR_1 and CR_2. In the second set of measurements with a second roof of absorber and two additional counters CR_3 and CR_4 placed on the top of the apparatus, as described in section II (see also Fig. 1), we have directly evaluated the fraction of e^+e^- events that were lost due to anticoincidence in CR_1 and CR_2. This was done by measuring the fraction, f, of "marked" e^+e^- events (i.e. not vetoed by CR_3 and CR_4, but in which CR_1 or/and CR_2 were triggered, see section II). Since the number of e^+e^- events vetoed by CR_3 and CR_4 was determined to be negligible, f represents directly the fraction of events lost in the first set of measurements, and was found to vary linearly from $f = 4.2\%$ at $E_+ = 0.725$ GeV to $f = 13.3\%$ at $E_+ = 1.2$ GeV (see Fig. 6). For the energies covered in the first set of measurements but not in the second, a linear linterpolation of f was used. The values of f and the correction factors $F_{AC} = (1-f)^{-1}$ we have used, are listed in columns (4) and (5) of Table III.

c) "Multiple scattering correction". - The geometrical acceptance is reduced by a small factor due to multiple scattering near the boundary of the telescopes. We have calculated the correction for these losses to be approximately energy independent and equal to $(+2.5 \pm 2)\%$.

d) "Geometrical misalignement correction". - Due to possible misalignements of the apparatus with respect to the source position, an uncertainty

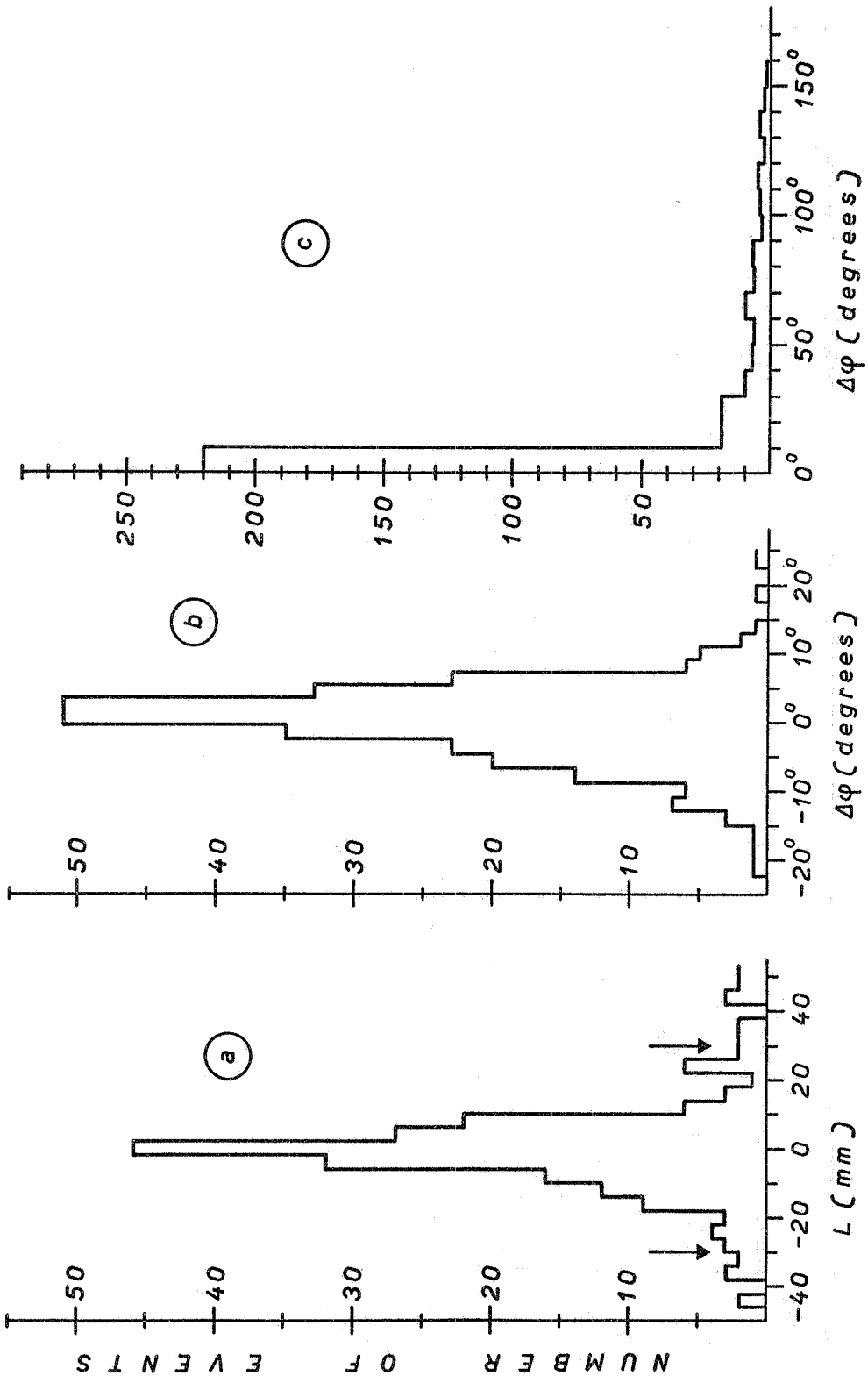

FIG. 5 - Track analysis of a sample of in-time $[\mu, e]$ events. a) L distribution; b) $\Delta\varphi$ distribution in the region around 0°; c) total $|\Delta\varphi|$ distribution.

is to be assigned to our geometrical acceptance. The corresponding correction to be applied to measured events is: $(+3 \pm 3)\%$.

TABLE III

Shower corrections and anticoincidence corrections. Col. 1, single beam energy; col. 2, ε_μ, measured shower inefficiency; col. 3, F_S shower correction factor; col. 4, f, measured fraction of "marked" events; col. 5, F_{AC}, anticoincidence correction factor.

$E_\pm$ (GeV) (1)	"Shower correction" ε_μ (%) (2)	F_S (3)	"CR veto correction" f (%) (4)	F_{AC} (5)
0.7	12.61 ± .34	1.31 ± .07		1.039 ± 0.17
0.725			4.2 ± .7	1.044 ± .018
0.75	7.94 ± .20	1.18 ± .06		1.049 ± .018
0.8	9.83 ± .24	1.23 ± .06		1.060 ± .015
0.825	8.33 ± .17	1.19 ± .05		1.066 ± .016
0.85	9.83 ± .20	1.23 ± .05		1.072 ± .017
0.875	8.71 ± .22	1.20 ± .06		1.078 ± .017
0.9	8.71 ± .18	1.20 ± .05		1.082 ± .020
0.925	6.34 ± .22	1.14 ± .08	8.2 ± 1.7	1.089 ± .020
0.95	7.15 ± .15	1.16 ± .05		1.094 ± .022
1.0	6.74 ± .15	1.15 ± .05		1.105 ± .024
1.20	4.65 ± .17	1.10 ± .08	13.3 ± 2.6	1.153 ± .035

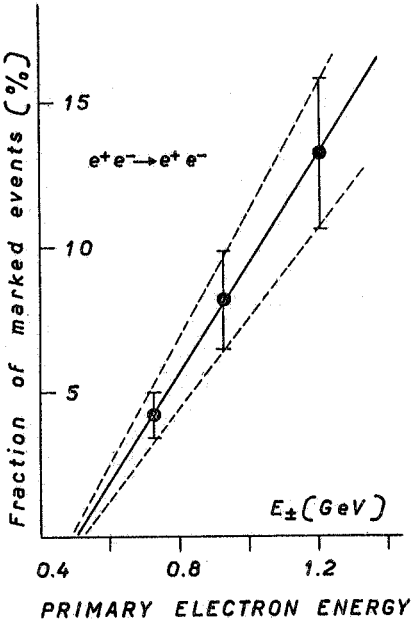

FIG. 6 - The fraction of "marked" [e, e] events as a function of the primary electron energy, $E_\pm$.

e) "Radiative corrections". Calculated radiative corrections turn out to be, in our case, quite negligible ($\lesssim 2\%$).

We summarize the situation on the corrections as follows:

a) Shower corrections: ranging from + 31% at 1.4 GeV $E_+ + E_-$ C.M. energy to + 10% at 2.4 GeV (experimentally measured);

b) CR veto corrections: ranging from + 3.9% at 1.4 GeV to 15.3% at 2.4 GeV (experimentally measured);

c) Multiple scattering correction: $(+2.5 \pm 2)\%$ (calculated value);

d) Geometrical misalignements correction: $(+3 \pm 3)\%$ (calculated value);

e) Radiative corrections: negligible ($\lesssim 2\%$, calculated value).

All of the above corrections have been applied to the number of collected events, after background subtractions have been performed. The corrected numbers of e^+e^- Bhabha scattering events are listed in column (6) of Table II. However the systematic uncertainties which are the same at all the energies (associated with multiple scattering and geometrical misalignements corrections) are not included in the quoted errors. They will be shown in the data display in Fig. 8 (along with the 5% energy indipendent monitor normalization uncertainty) as an overall normalization uncertainty around the theoretical prediction.

IV.4. - Comparison with theory. -

According to QED, the elastic electron-positron scattering is described at the lowest order by the graphs shown in Fig. 7.

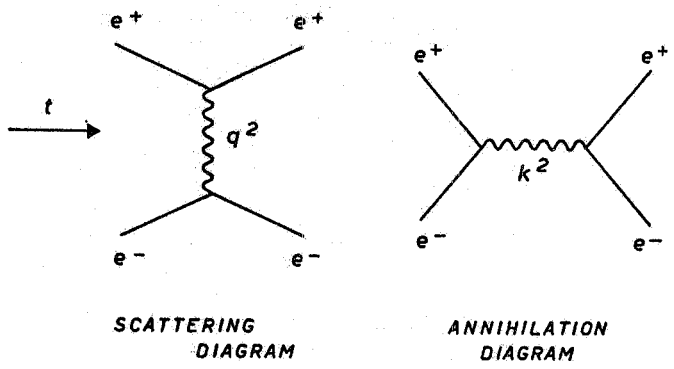

FIG. 7 - Feynmann diagrams for e^+e^- elastic scattering at lowest order.

The four-momentum squared of the virtual photon is space-like in the scattering graph and time-like in the annihilation graph. In the C.M. system they are respectively given by:

$$q^2 = +4E_{\pm}^2 \sin^2 \theta/2 \qquad \text{and} \qquad k^2 = -4\, E_{\pm}^2,$$

where E_+ is the energy of either the electron or the positron and θ is the scattering angle.

The resulting cross-section (Bhabha cross-section) can be written as:

$$(IV.1) \qquad \left(\frac{d\sigma}{d\Omega}\right)_{\text{Bhabha}} = \frac{r_o^2}{8}\left(\frac{m_e}{E_{\pm}}\right)^2 \left[S(q^2,k^2)+I(q^2,k^2)+A(q^2,k^2)\right]$$

where: m_e and r_o are the mass and the classical radius of the electron;

$$S(q^2,k^2) = \frac{k^4+(q^2+k^2)^2}{q^4}$$

is the contribution of the scattering graph;

$$A(q^2,k^2) = \frac{q^4+(q^2+k^2)^2}{k^4}$$

is the contribution of the annihilation graph and

$$I(q^2,k^2) = 2\,\frac{(q^2+k^2)^2}{k^2 q^2}$$

is the interference term between the two graphs.

Of course, the Bhabha formula is only a first order description of the electron-positron scattering process and we must consider terms from higher order diagrams, that is

$$(\frac{d\sigma}{d\Omega})_{QED} = (\frac{d\sigma}{d\Omega})_{Bhabha} + \text{Radiative corrections.} \qquad \text{(IV.2)}$$

These radiative corrections can be separated into virtual (internal) and real (external) photon contributions whose divergent parts cancel to order α^3[17]. These contributions have been calculated for wide angle electron-positron scattering[18], and for our apparatus result in a small corrections ($\lesssim 2\%$) due to the compensation of internal and external contributions, each of which is in some cases as large as 10%.

Experimentally we wish to verify whether or not the e^+e^- elastic scattering is actually described by the point-like elastic scattering cross-section $(d\sigma/d\Omega)_{QED}$. We have therefore considered the ratio (R_{exp}) of the experimentally measured cross-section to the point-like cross section integrated over our angular acceptance $\Delta\Omega$:

$$R_{exp} = \frac{\int_{\Delta\Omega} (d\sigma/d\Omega)_{exp}\, d\Omega}{\int_{\Delta\Omega} (d\sigma/d\Omega)_{QED}\, d\Omega} \qquad \text{(IV.3)}$$

Of course if the scattering process is actually described by the point-like cross-section, this ratio will be 1.

In order to be able to interpret any deviations of R_{exp} from 1 we will consider the most general form (at the 1st order) that can be assumed for a non-point-like elastic scattering cross-section consistent with Lorentz and Gauge invariance. Taking into account that the electron anomalous magnetic moment μ_a is small ($\mu_a/m_e \ll e$[19]) we can write

$$(\frac{d\sigma}{d\Omega})_{Modified} = \frac{r_o^2}{8}\left(\frac{m_e}{E_{\pm}}\right)^2 \Big[|G(q^2)|^2 S(q^2,k^2) + \qquad \text{(IV.4)}$$

$$+ \mathrm{Re}(G(q^2)G^*(k^2))\, I(q^2,k^2) + |G(k^2)|^2 A(q^2,k^2) \Big]$$

where $G(q^2) = F^2(q^2)\,M(q^2)$ is the product of a possible electron form factor squared $F^2(q^2)$ and a possible modification factor ($M(q^2)$) to the photon propagator. For our

apparatus centered around $\theta = 90^{o}$ the contribution from the scattering term dominates that of the interference and annihilation terms. In this case and if we neglect the radiative correction contribution which has been shown to be small in the point-like case, we find $R_{exp} \simeq \langle |G|^2 \rangle$. $\langle |G|^2 \rangle$ is the weighted average of $|G|^2$ over the experimental apparatus. Clearly a test of the validity of QED (i.e. $|G|^2 = 1$) is therefore equivalent to verify that $R_{exp} \equiv 1$, while a measurement of this ratio different from 1 can directly be associated with the average value of the form factor $\langle |G|^2 \rangle$.

We can now rewrite the equation (IV.3) in terms of the detected wide angle scattering events, $n_{e^+e^-}$, and the monitor events, m (see section III), as follows:

$$(IV.5) \qquad R_{exp} = \frac{n_{e^+e^-}}{\mathcal{L}} \Big/ \int_{\Delta\Omega} \left(\frac{d\sigma}{d\Omega}\right)_{QED} d\Omega = \frac{n_{e^+e^-}}{m} \frac{\int_M \left(\frac{d\sigma}{d\Omega}\right)_{QED} d\Omega}{\int_{\Delta\Omega} \left(\frac{d\sigma}{d\Omega}\right)_{QED} d\Omega}$$

The last step makes use of the determination of the integrated luminosity, $\mathcal{L}$, through the measurement of the yield m in the monitor apparatus, M[19 bis], i.e.

$$(IV.6) \qquad m = \mathcal{L} \int_M (d\sigma/d\Omega)_{QED} \, d\Omega$$

where we have made the hypothesis that e^+e^- scattering is well described by QED (point-like) at the small momentum transfers involved in the monitor apparatus. Again, in the case of the monitor, radiative corrections to the Bhabha cross-section have been calculated[20] and are found to be small ($< 2\%$).

Expressing R_{exp} as a ratio of wide angle events to monitor events minimizes the sensitivity of our results to the actual value of the finite, energy dependent, source length $\bar{l}_z$ (Ref. (9), section II) since the efficiencies of both the monitor and our experimental apparatus have approximately the same dependence on $\bar{l}_z$. Additional care must be taken in the evaluation of (IV.5) to symmetrize the QED cross section in θ and $\pi - \theta$ since our apparatus does not permit charge recognition.

The results of the evaluation of R_{exp} for each measured C.M. energy are shown in Fig. (8). The statistical errors for each point are shown as bars, while the systematic, energy dependent, uncertainties due to erratic fluctuations in the monitor ($\pm 7\%$) are indicated as small rectangles. The systematic uncertainties due to multiple scattering corrections ($\pm 3\%$), geometrical misalignement ($\pm 3\%$), and over all monitor normalization ($\pm 5\%$), have been indicated by a dashed band (± 6.5) centered about $R_{exp} = 1$. In the same figure is also shown the q^2 acceptance $n(q^2)$ of the apparatus, weighted on the Bhabha cross-section.

Our data do not indicate any deviation from $\langle |G(q^2)|^2 \rangle = 1$ over the range of q^2 explored and they are fitted very well ($\chi^2 = 10.8$ for 10 degrees of freedom) by an horizontal straight line

$$\bar{R}_{exp} = 1.05 \pm 0.04 \; (\pm 6.5\% \text{ systematic})$$

which is to be compared to the point-like prediction $R = 1.00$[20 bis].

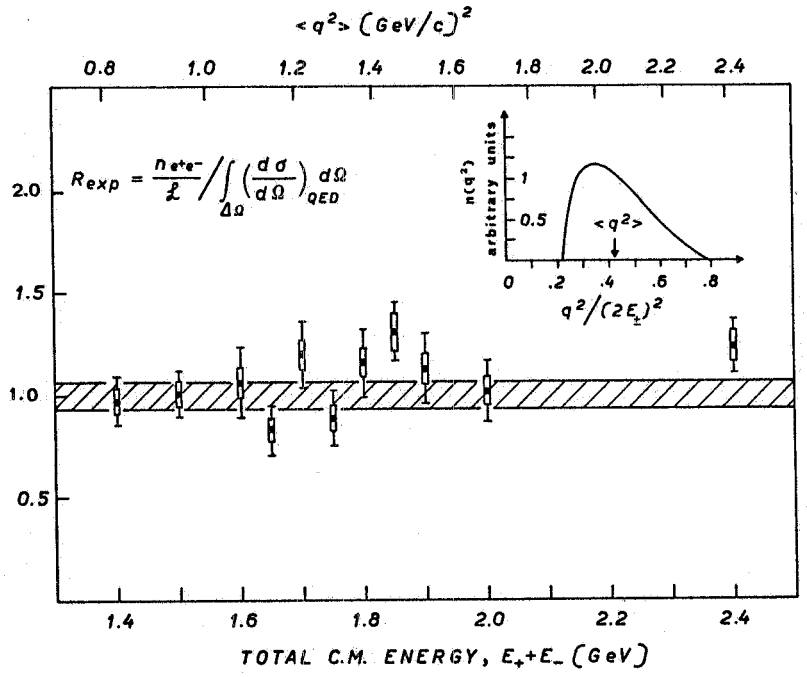

FIG. 8 - Wide angle e^+e^- elastic scattering data compared, as a function of the total C.M. energy with QED theory. For each experimental point statistical errors are shown as bars, while systematic uncertainties are indicated as small rectangles. The dashed band ($\pm 6.5\%$) about $R_{exp} = 1.0$ indicates the systematic uncertainties which are the same at all the energies. The q^2 acceptance of the apparatus weighted on the Bhabha cross-section is shown in the upper right hand corner.

V. - REACTION $e^+e^- \rightarrow a^\pm + b^\pm +$ ANYTHING. -

V.1. - Selection of the events. -

We will now discuss events from the reaction

$$e^+e^- \rightarrow a^\pm + b^\pm + \text{anything.} \qquad \text{(V.1)}$$

where $a^\pm$ and $b^\pm$ are any charged particles. The master coincidence which triggers the apparatus requires the presence of at least two charged particles ($a^\pm$ and $b^\pm$) detected in two different telescopes.

Since reaction (V.1) is not a two body reaction we have restricted ourselves to the analysis of "non-coplanar" events, which are defined as follows:

a) more than two charged particles detected each entering a different telescope, and having a pulse height $H_i \geq H_{i,\,min}$;

b) only two charged particles detected but with the restrictions that their pulse heights (H_i, H_j) (greater than the respective low pulse height cuts $H_{i,\,min}$ and $H_{j,\,min}$) are not in the region [e, e] of the pulse height plot (see Fig. 3 for reference); and further their non-coplanarity angle $|\Delta\varphi|$ (defined in Ref. (15), section IV.1) is $\geq 13^\circ$;

c) only two charged particles are detected but their pulse heights are in the [e, e] region of the pulse height plot and the non-coplanrity angle $|\Delta\varphi| \geq 40^\circ$.

Selection criterion c) was chosen in order to exclude from our sample any contamination from the radiative reaction $e^+e^- \rightarrow e^+e^-\gamma$. However, the number of the non-coplanar events selected with criterion c) was only a small fraction ($\sim$7%, see section V.2) of the observed non-coplanar events.

The evaluation of the non-coplanarity angle ($\Delta\varphi$) between 2 particles requires information on the projected paths of the particles and therefore the positions of the sparks in both monogap, magnetostrictive chambers of the two telescopes traversed by the particles. An event with this complete determination of track positions is designated here after a "4-chamber" event or "4-chm". Since our monogap spark chambers have an efficiency of $\sim$85% (see Ref. (16), section IV.1), confining ourselves to "4-chm" events rejects $\sim$50% of all the events. We will see however, that we can analyze those events in which the spark in one of the four chambers is missing ("3-chamber" events, or "3-chm") by making an additional hypothesis. The analysis of these "3-chm" events has been performed and is presented after that of the "4-chm" events.

For completeness, we recall (see section II) that we have performed two different sets of measurements. During the first set the counters CR_1, CR_2 were used as veto counters in the trigger; in the second set of measurements, counters CR_3, CR_4 were added and used as veto counters while counters CR_1, CR_2 were only recorded. In order to have an homogeneous set of data we do not include in the following analysis events in which a particle crosses the 22 cm Fe and stops in the lead absorber between CR_1, CR_2 and CR_3, CR_4 ("marked" events). We have used the number of detected "marked" events to obtain information on the penetration of the detected particles.

V.1.1. - 4-chamber events. Analysis and background subtractions. -

These events are defined as those for which the projection on a plane orthogonal to the beam axis of the tracks of at least two charged particles are completely determined. That is, by definition in a "4-chm" event a complete reconstruction is possible for at least two charged particle trajectories (if other particles are present in other telescopes their track reconstruction may or may not be possible). For each of the reconstructed tracks the minimum distance from the beam axis (L_i) and the azimuthal angle (φ_i) (see Section II) can be evaluated. Using the azimuthal angles we can select the non-coplanar "4-chm" events.

Among these events, those from reaction (V.1) must occur in-time with the beam-beam impact. From the analysis of the Bhabha events we have already determined the "in-time" interval, Δt (see Fig. 4, section IV.1).

In addition these events must originate in the region of intersection of the electron-positron bunches ("source region"). Therefore we have studied the distribution of the distances from the beam axis of the detected particle tracks.

In Fig. 9 a bidimensional sample plot of non-coplanar events in a plane L_i, L_j is presented. Fig. 9(a) refers to in-time events, and shows a clear clustering of events about the origin (projection of the beam axis) in addition to a cosmic ray and machine background scattered over the entire plane. Fig. 9(b) shows the same plot for a sample of out-of-time events. In this case a clustering near the origin is not present since the out-of-time events are cosmic rays.

In Fig. 10(a) we have projected the plot of Fig. 9(a) on the L_i axis. There is a clear peak of events coming from the source. A smooth interpolation un

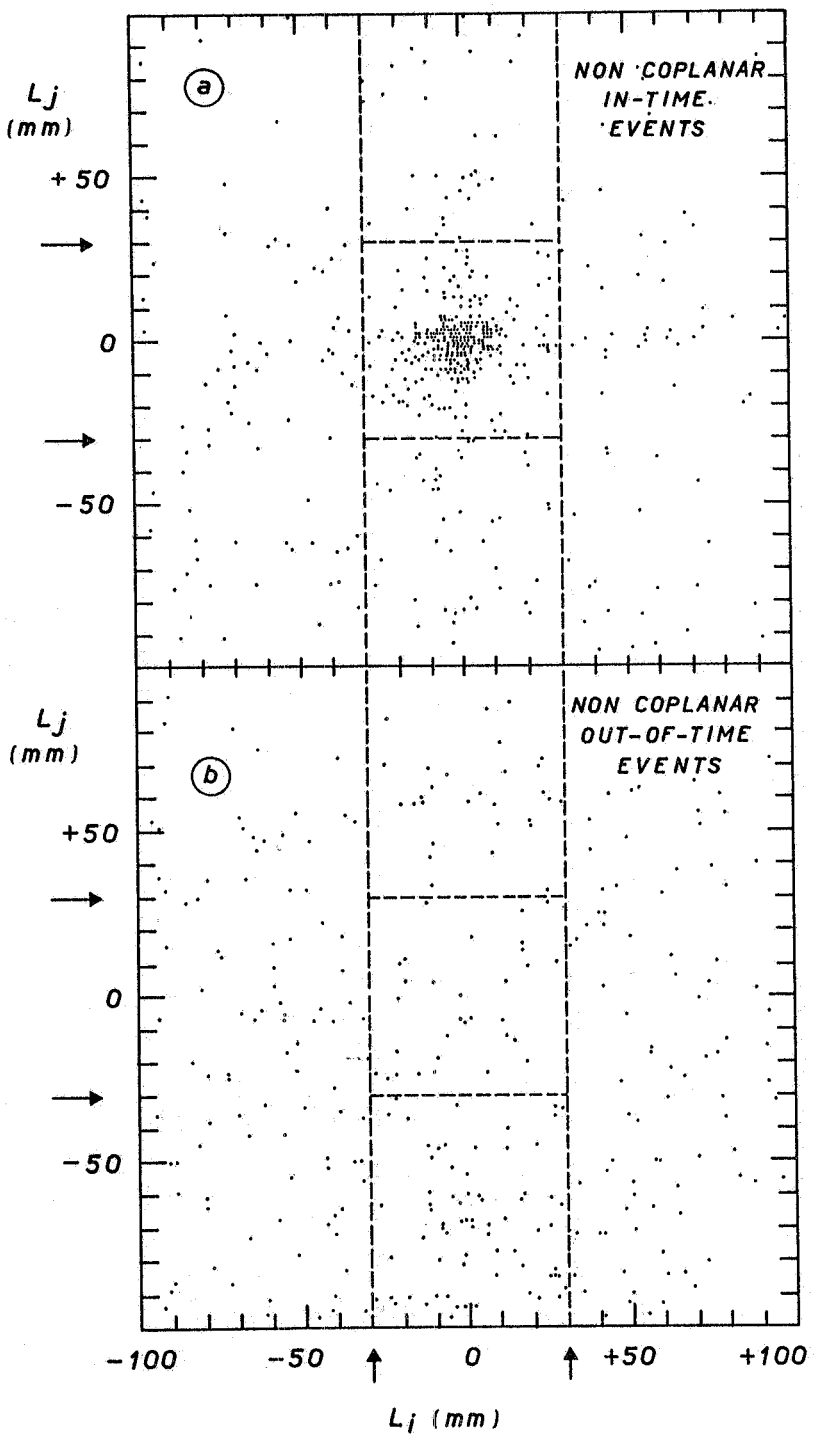

FIG. 9 - Plots of L_i versus L_j for a sample of "4-chamber" non-coplanar events. a) In-time events; b) Out-of-time events.

der the peak of the background tails would indicate a background contamination of roughly 20% to the events coming from the source. However, if we project on the L_j axis those events for which $|L_i| \leq 30$ mm , (Fig. 10(b)),the peak of the events from the source is now superimposed over a somewhat smaller background (interpolated value ~10%). As was the case for the Bhabha events the source width (~7.5 mm) is what one would expect from spark chamber resolution and multiple scattering in the vacuum chamber walls and telescope absorbers. From the analysis of these type of distributions, we have defined as in-source events those for which $|L_i|$ and $|L_j|$ are both ≤ 30 mm.

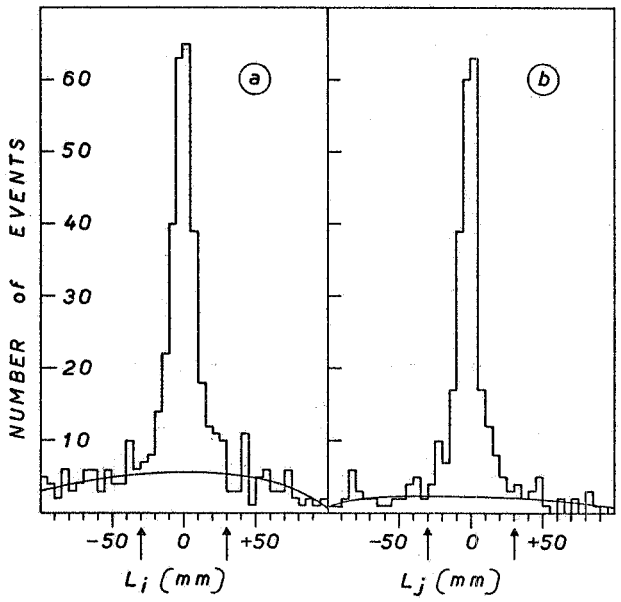

FIG. 10 - Projections of the sample plot in Fig. 9(a). a) All the events projected on the L_i axis; b) The events for which $L_i \leq 30$ mm, projected on the L_j axis.

Fig. 11(a) shows the L_j distribution (equivalent to the distribution of Fig. 10(b)) for all our "4-chm", non-coplanar, in-time events. The Δt distribution in Fig. 11(b) for the "4-chm", non coplanar; in-source events clearly demonstrates that practically all the events are in-time with the beam impact.

We have collected in the energy range $E_+ + E_- = 1.4 - 2.4$ GeV, a total of 428 "4-chm" non-coplanar events which are in-time with the beam-beam impact and come from the source region. These events are listed in column (2) of Table IV and are divided according to their detected configuration: i.e. two charged tracks detected (2τ, following the notations of section II); two charged plus one neutral ($2\tau + \mathcal{N}$); etc.

From these events we must subtract cosmic ray and machine associated background. Since the machine background will be peaked in the source region due to beam-gas interactions, a smooth interpolation of the background tails of the L distribution is not a correct procedure to determine the total background contamination of the in-source events.

The cosmic ray contribution to the in-time, in-source, non-coplanar events can be calculated at each energy by appropriately normalizing the corresponding out-of-time events. The normalization factor was determined from the ratio of in-time to out-of-time events during machine-off background runs. The cosmic ray contamination for these "4-chm" events was quite small at all

energies, the average being $\sim 2.5\%$. The cosmic ray subtraction for each configuration is listed in column (3) of Table IV.

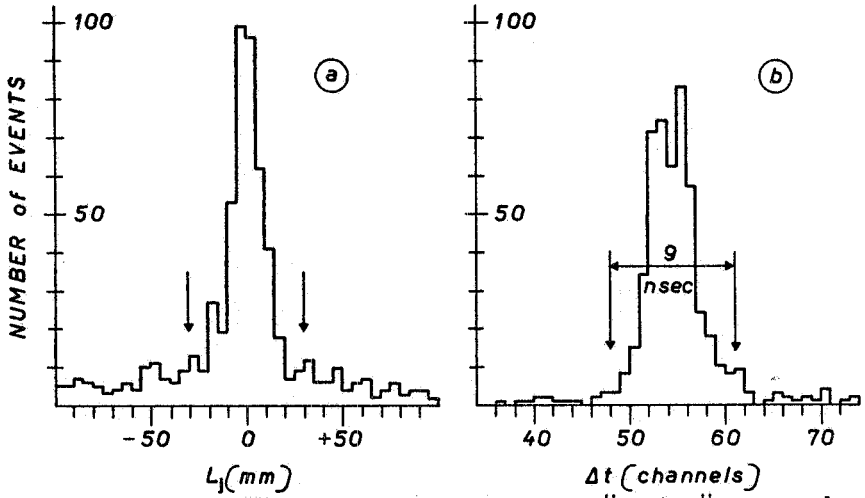

FIG. 11 - L_j and Δt distributions for all the "4-chm" non-coplanar events. a) L_j distribution for the in-time events for which $L_i \leq 30$ mm; b) Δt distribution for in source ($|L_i|, |L_j| \leq 30$ mm) events.

The amount of machine associated background was determined by background runs with one beam or two separated beams in the storage ring (see Section IV.2b). During 600 hours of these runs we collected 43 events which satisfied the selection criteria for non-coplanar events. After cosmic ray subtraction, we we normalized these events for each energy to our measurement runs, as was discussed in the case of wide-angle e^+e^- measurements. The average contamination of the in-source, in-time events due to these machine associated events was $23 \pm 4\%$. Practically all of this background was in the 2τ event configurations (see column (4), Table IV). As a function of C.M. energy this contamination was approximatly constant and $\leq 5\%$ in the energy range 1.4 - 1.9 GeV, but increased sharply to a maximum of $\sim 75\%$ at 2.4 GeV.

After cosmic ray and machine background subtractions, the total number of non-coplanar "4-chm" events is 317 and they are listed by configuration in column (5), Table IV.

As a final remark, we note that with the normalization procedures used for the background subtractions, (within the statistical errors) we can account for all of the out-of-source events in the tails of the L distribution (see Fig. 11(a)).

V.1.2. - "3-chamber" events. - Analysis and background subtractions. -

For these events only one charged particle trajectory is completely defined by a spark in both chambers of the triggered telescope T_i. The second (and possible the third) particle trajectory is not completely determined, since a spark is missing in one chamber of it's telescope T_j. In order to determine the trajectory of this second (third) particle we make the hypothesis that the event originates at that point of the trajectory, measured in telescope T_i, which is closest to the beam axis. In this way we can determine the azimuthal angle (φ_j) for the particle trajectories with only one spark.

TABLE IV

List of "4-chm" and "3-chm" non-coplanar events and background subtractions for the various detected configurations.

	4-chamber non-coplanar events				3-chamber non-coplanar events				4 chamber + +3 chamber non-coplanar events, after background subtractions (10)
Detected configuration (1)	Collected events (2)	Normalized cosmic ray background (3)	Normalized beam-gas background (4)	Non-coplanar events after background subtractions (5)	Collected events (6)	Normalized cosmic ray background (7)	Normalized beam-gas background (8)	Non-coplanar events after background subtractions (9)	
2τ	333	8.4 ±1.6	95.6±15.0	229.0±24.0	513	133.8±6.7	157.2±21.7	222.0±32.0	451.0±40.0
$2\tau + 1\mathcal{N}$	49	0.6 ± .4	4.8± 3.3	43.6±7.8	59	11.1±1.9	11.9± 5.9	36.0± 9.9	79.6±12.6
$2\tau + 2\mathcal{N}$	3	0.0 ± .35	0.0± 2.0	3.0±2.7	8	0.8±0.7	3.3± 2.0	3.9± 3.5	6.9± 4.4
3τ	39	1.1 ± .6	0.0± 2.0	37.9±6.6	25	5.4±1.2	-3.8± 2.4	23.4± 5.7	61.3± 8.7
$3\tau + 1\mathcal{N}$	4	0.0 ± .35	0.0± 2.0	4.0±2.9	4	0.6±0.5	0.8± 2.0	2.6± 2.9	6.6± 4.1
Totals	428	10.15±1.9	100.4±16.0	317.5±26.0	609	151.7±7.2	169.4±23.0	287.9±34.3	605.4±43.1

The resulting uncertainty in the determination of φ_j is quite small ($\delta\varphi_j < 2^o$) for those events physically originating in the source region. On the other hand some events physically originating outside the source region, which are due to C.R. and machine background, by this procedure can be added to our sample of in-source events. In fact the reconstructed origins of the "3-chamber" events are closer to the beam axis than the "true" origins. Therefore this procedure will result only in a larger background contamination to be subtracted from our "3-chamber" events.

The analysis of the "3-chm" events can then procede as for "4-chm" events. The only difference is that L_i vs L_j bidimensional plots cannot be compiled. However, it is possible to construct the one-dimensional distribution of events as a function of L_i without any condition on L_j (which is not measured). This distribution, which is the equivalent of the one shown in Fig.10(a) for "4-chm" events, is given in Fig. 12(a). The "in-source" 3-chm" events are now defined as those for which $|L_i| \leq 30$ mm. By comparing the L distribution of Fig. 11(a) ("4-chm" events) with Fig. 12(a), we confirm that this analysis of the "3-chm" events simply results in a somewhat higher background contamination. Fig. 12(b), which shows the Δt distribution for the "3-chm" non-coplanar events coming from the source, allows us to conclude that most of the additional background is due to cosmic rays.

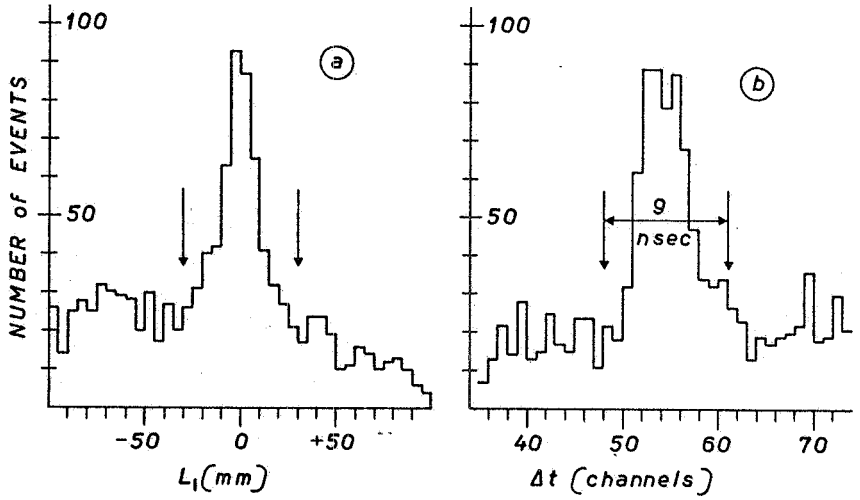

FIG. 12 - L_j and Δt distributions for all the "3-chm" non-coplanar events. a) L_i distribution of the measurable track for in-time events; b) Δt distribution for in-source events.

We have collected a total of 609 "3-chm" events which are non-coplanar, in-time with the beam-beam impact and come from the source. They refer to several C.M. energies between 1.4 and 2.4 GeV and are listed in column (6) of Tab. IV according to their detected configurations.

Background subtractions from the "3-chm" events have been performed in the same way as for the "4-chm" events. Cosmic rays contamination has been evaluated by selecting and appropriately normalizing the "3-chm" out-of-time events. This cosmic rays contamination ranges from 17% at 2.4 GeV to 40% at 1.4 GeV, the average contamination being ~25%. The machine background to be subtracted the "3-chm", in-time, in-source, non-coplanar events has been measured to have the same value within the errors, energy by energy, as for the

"4-chm" events (average value 28 ± 4%). Cosmic ray and machine background subtractions, for the "3-chm" events are listed in coulmns (7) and (8) of Table IV

The remaining 288 non-coplanar "3-chm" events we are left with after background subtractions, are listed in column (9) of Table IV according their different detected configurations.

V.2.- Nature of the observed particles.-

From the analysis we have discussed in the previous sections and after we have subtracted the C.R. and machine background, there remain (see column (10) of Table IV) with a total of 605("3-chm"+"4-chm") events, which are non-coplanar, originate in the source region, and are in-time with the beam--beam impact, i.e. they come from the reaction

$$e^+e^- \rightarrow a^{\pm} + b^{\pm} + \text{anything}.$$

In this section we will discuss the nature of the produced particles. The information made available by our apparatus is not sufficient to determine the nature of each individual detected particle. However some statistical information can be extracted by the experimental distributions.

First, we have the pulse height information from the sandwich counters (C_i+D_i). In Figs. 13(a) and (b) pulse height spectra of the charged particles τ_1 detected in telescope T_1 are shown (within the errors the distributions in the other telescopes are the same). The pulse height spectrum of particles associated with the detected non-coplanar events (Fig. 13(b)) is compared with the spectrum of minimum ionizing particles (C.R.) and high energy electrons from Bhabha scattering (Fig. 13(a)). The distribution of the non-coplanar events is quite similar to the C.R. spectrum although it shows a non-negligible tail towards the larger pulse heights. However, by compiling the two dimensional plot H_j vs H_i for the in-time, non--coplanar events coming from the source, we have checked that the great majority of the events (~93%) does not show any correlation between large pulse heights in the different telescopes. In fact (using the definitions of section IV.1, see Fig. 3 for reference) 61% of the events have their pulse heights (H_i, H_j) in the $[\mu, \mu]$ region of the pulse height plot, 32% in the $[\mu, e]$ region and only ~7% in the $[e, e]$ region. These percentages correspond to the ~19% large pulse height tail in the non-coplanar event distribution of Fig. 13(b). A large fraction of this tail is due to the presence of more than one particle in the same telescope. Actually, from the experimental numbers of events with more than two detected particles (see Tab. IV) we can estimate this fraction to be ~14%.

Moreover, if the detected particles were pions, the remaining 5% of events in the tail could be easily accounted for due to the following effects: nuclear interactions in the sandwich counters and the possibility that the detected particles are low energy pions. We conclude that the bulk (> 95%) of the detected particles are not high energy electrons, and that the pulse height spectrum is compatible with all of them being pions.

Independent experimental information on the nature of the detected particles is obtained by measuring their penetration through the 22 cm Fe absorber on top of the apparatus. In Fig. 13(c) we have plotted, as a function of the primary electron energy $E_{\pm}$, the fraction f_M of the background subtracted non-coplanar events in which a particle crosses the 22 cm Fe and stops between CR_1,

CR_2 and CR_3, CR_4("marked"events). In the same figure the fraction of"marked" Bhabha electrons (see Sect.IV.3) is also plotted. The number of'marked'Bhabha event decreases to zero at low energy and we can thus conclude that electrons with energy smaller than 500 MeV have a negligible probability ($< 1\%$) to cross the Fe absorber and to give a mark. On the other hand, the fraction f_M of"marked" non-coplanar events does not appear, within the large errors, to have a strong energy dependence, it's average value being $(16 \pm 4)\%$. To give a feeling for such a figure, we have calculated as 16% the probability of a ~400 MeV pion entering one of the top telescopes to be marked. Furthermore, we have performed a Montecarlo calculation (see Appendix A) which shows that, at $E_+ = 0.7$ GeV, no reasonable pion final state would result in a value of f_M greater than 16%. This indicates that at 1.4 GeV C.M. energy the possible contamination of low energy (< 500 MeV) electrons must be very low. Also at the higher energies the measured values of f_M are consistent with a major part of the detected particles being pions.

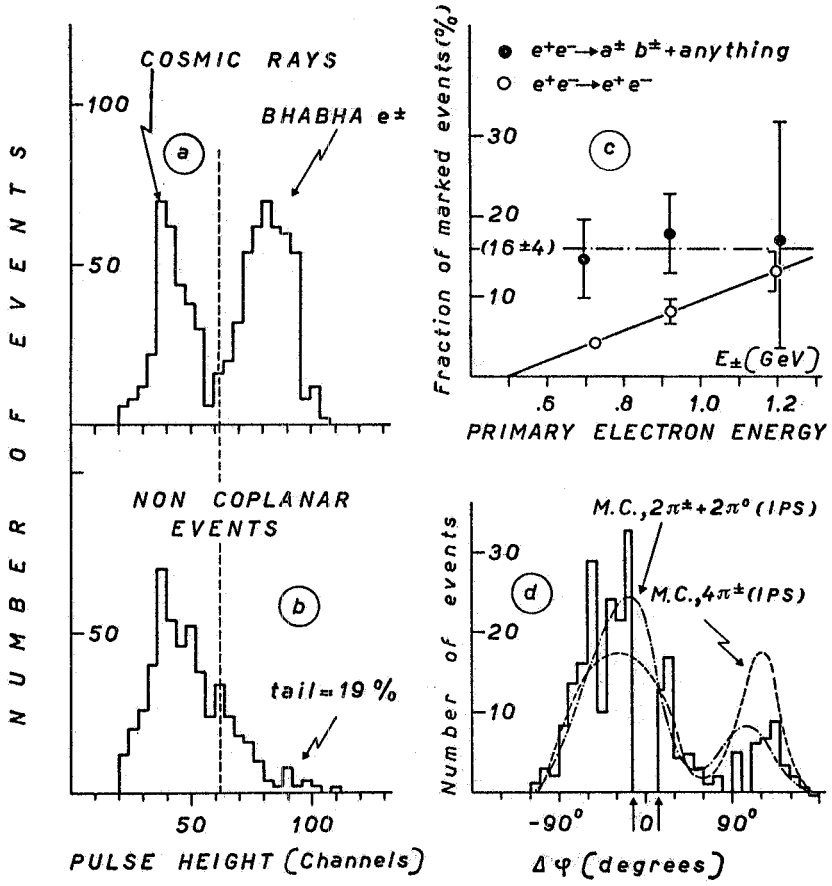

FIG. 13 - a) Cosmic ray and Bhabha electrons pulse height spectra in telescope T_1; b) pulse height distribution of in-time, in source, non-coplanar events in telescope T_1; c) fraction, f_M, of "marked" non-coplanar and Bhabha events; d) $\Delta\varphi$ distribution of the background subtracted "4-chm" non-coplanar events compared with an invariant phase space (IPS) Montecarlo calculation for two possible pion final states.

As will be discussed in section V.4, the experimental values of f_M will be used as one of the parameters of our best fit procedure in order to extract information on the relative contribution from the possible different production channels.

Additional information on the nature of the particles associated with the detected non-coplanar events can be obtained from the distribution of the $\Delta\varphi$ (non-coplanarity) angle.

In Fig. 13(d) the $\Delta\varphi$ distribution of the "4-chm" non-coplanar events is shown (the "3-chm" non-coplanar events have a similar $\Delta\varphi$ distribution). It is worth while to note that this distribution is not symmetric with respect to $\Delta\varphi = 0$. This is only due to our definition of the $\Delta\varphi$ sign, which was chosen (see Ref. (15), Section VI.1) in order to be directly related to the actual geometrical configuration of the event[21].

For reference we have also plotted in Fig. 13(d) the statistical $\Delta\varphi$ distribution expected for the reactions $e^+e^- \rightarrow \pi^+\pi^-\pi^0\pi^0$ and $e^+e^- \rightarrow \pi^+\pi^-\pi^+\pi^-$ (phase-space Montecarlo calculation, see Appendix A). The general features of the experimental $\Delta\varphi$ distribution is quite similar, especially around $\Delta\varphi = 0$, to the statistical ones. That is, the $\Delta\varphi$ distribution of non-coplanar events is compatible with some admixture of final states produced with a statistical angular distribution. In section V.4 we will discuss this point in a more quantitative way.

Here we are mainly concerned with the hadronic nature of the detected particles and we use the $\Delta\varphi$ distribution in order to conclude that our sample of non-coplanar events does not contain a significant contribution from a particular non hadronic process, namely

(V.2) $$e^+e^- \rightarrow e^+e^-e^+e^-.$$

Actually this is the only plausible process which could produce low energy non-coplanar electrons, and it is foreseen to occur, at a relatively high rate, through the diagram shown in Fig. 14.

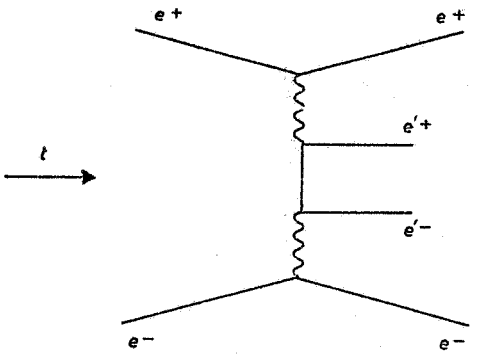

FIG. 14 - Two photon interaction diagram for the reaction $e^+e^- \rightarrow e^+e^-e^+e^-$.

According to this diagram, the e^+ and e^- in the final state are scattered in a small cone around the beam direction, while the produced e'^- and e'^+ have a peculiar $\Delta\varphi$ distribution, since the $d\sigma/d(\Delta\varphi)$ for this reaction is strongly peaked around $\Delta\varphi = 0$ ($\Delta\varphi$ being the non-coplanarity angle between e'^- and e'^+). In Fig. 15(b) we have plotted the cross section $d\sigma/d(\Delta\varphi)$ of our non-coplanar events ($|\Delta\varphi| \geq 13^o$). This was obtained as a ratio between the experimental distribution of Fig. 13(d) and the geometrical detection efficiency of our apparatus, $\varepsilon_g(\Delta\varphi)$, to detect a two track configuration with relative

non-coplanarity angle $\Delta\varphi$. The experimental values of $d\sigma/d(\Delta\varphi)$ appear to be quite constant, within the errors, proving that the contribution from the reaction $e^+e^- \rightarrow e^+e^-e^+e^-$ does not extend, with appreciable tails, outside the region $|\Delta\varphi| < 13^o$. In Fig. 15(a) we have indicated the theoretical cross-section shape for the reaction (V.2) calculated according to Baier and Fadin[22]. When normalized to give the maximum 13^o peaking possible within our indicated errors, this curve allows at most a 10% contamination to our sample of non-coplanar events.

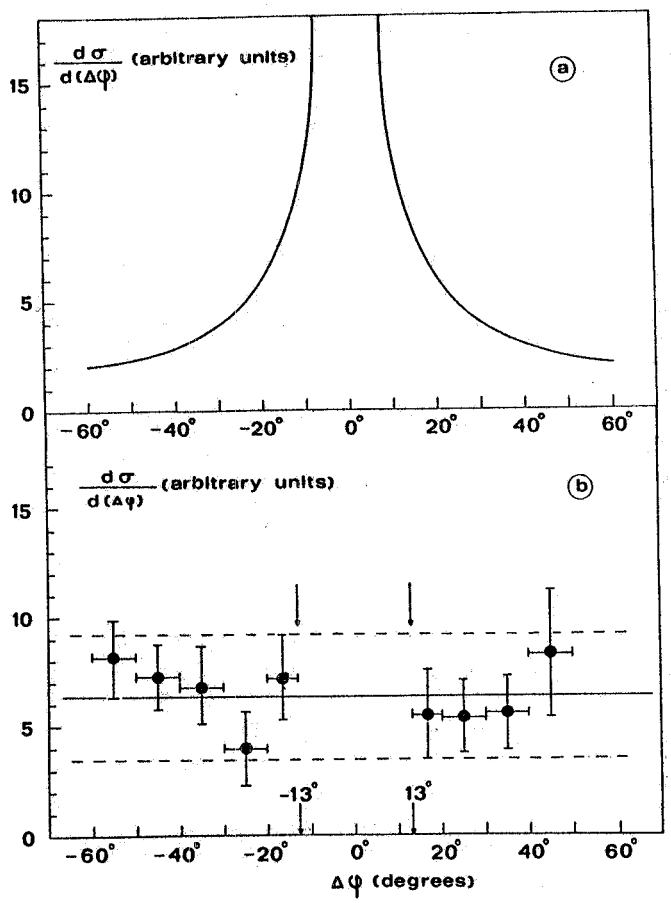

FIG. 15 - a) Theoretical shape of $d\sigma/d(\Delta\varphi)$ for the reaction $e^+e^- \rightarrow e^+e^-e^+e^-$, according to Baier and Fadin[22]; b) $d\sigma/d(\Delta\varphi)$ calculated from the experimental $\Delta\varphi$ distribution of in-time, in-source non-coplanar events.

We can not only exclude a large contamination (for $|\Delta\varphi| \geq 13^o$) from the reaction $e^+e^- \rightarrow e^+e^-e^+e^-$, but from similar considerations, we can set an upper limit of ~ 10% for the total possible contamination from processes with a $\Delta\varphi$ distribution strongly peaked around $\Delta\varphi = 0$; i.e. $e^+e^- \rightarrow e^+e^- \mu^+\mu^-$, $e^+e^- \rightarrow e^+e^- \pi^+\pi^-$ [23] etc.

We summarize the conclusions of this section as follows. The detected particles associated with our non-coplanar events originating from the reaction $e^+e^- \rightarrow a^\pm + b^\pm +$ anything are of hadronic nature, ~10% being an upper li-

mit for a possible contamination of electrons. In addition also the contribution from the reaction $e^+e^- \rightarrow a^{\pm}b^{\mp} + e^+e^-$ via two photon annihilation appears to be very small.

V.3. - Corrections to the data and list of the events from the reaction $e^+e^- \rightarrow a^{\pm} + b^{\pm}$ + anything. -

As we have already remarked, the 605 background subtracted non-coplanar events detected by our apparatus (which are listed by configurations in column (10) of Table IV) originate from the reaction

(V.1) $$e^+e^- \rightarrow a^{\pm} + b^{\pm} + \text{anything}$$

Several corrections must now be applied to these experimental data in order to obtain the total number of events which were produced through the above reaction (V.1).

First, many events with only two detected charged tracks (i.e. the detected configurations 2τ, $2\tau + \mathcal{N}$, $2\tau + 2\mathcal{N}$), were rejected because of the non-coplanarity cut in $\Delta\varphi$. We recall that the non-coplanarity cut was set at 13^o for events selected according to criterion b) of section V.1 (93% of the detected events with two charged tracks); while $|\Delta\varphi| \geq 40^o$ was required for the events satisfying the selection criterion c) ($\sim 7\%$ of the total). The corresponding correction has been determined by a smooth interpolation between $-13^o < \Delta\varphi < +13^o$ ($-40^o < \Delta\varphi < +40^o$) of the experimental $\Delta\varphi$ distribution, which, we have seen, is consistent with a statistical angular distribution (see section V.2 for reference). The overall $\Delta\varphi$ cut correction to be applied to the 451 2τ detected events was measured to be $(+18 \pm 3)\%$, the correction to the 80 $2\tau + \mathcal{N}$ detected events is $(+12 \pm 2)\%$; and it is negligible for the $2\tau + 2\mathcal{N}$ configuration.

Further corrections are due to: losses due to the energy (range) cuts of the apparatus; nuclear interactions (absorption) of the produced particles; particles crossing the 22 cm Fe absorber and giving an anticoincidence signal pulse in the CR veto counters; and finally multiple scattering. These corrections depend on the nature and the energy distribution of the emitted particles, i.e. on the particular physical channel through which the particles are produced. Therefore these effects have been taken into account in the calculation of the detection efficiency of the apparatus performed with a Montecarlo program according to each considered final state. (see Appendix A).

A final small effect, due to the fact that our monogap spark chambers are not 100% efficient, has also been included in the Montecarlo calculation. In fact it affects essentially the relative distribution of the events between the different detected configurations and thus depends on the actual produced channels. Therefore the only correction applied directly to the numbers of events, is the $\Delta\varphi$ cut correction, all the other effects being taken into account in the efficiency calculation. The corrected numbers of events are listed in Table V for each C.M. energy, according to their different detected configurations. Table V contains also, in parenthesis, the raw numbers of in-time, non-coplanar events coming from the source ("4-chm"+"3-chm" events). In column (3) of Table V we give the numbers of wide angle Bhabha scattering events simultaneously collected in our apparatus. They are the sum of "4-chm" and "3-chm" events (according to the definition of section V.1) and, after background subtractions, have been corrected for all the effects listed in section IV.3. Once the validity of QED has been established, the wide angle Bhabha scattering reaction can be used to determine

TABLE V

List of background subtracted, in-time, in-source non-coplanar events according to their detected configuration, at the various energies, after the $\Delta\varphi$ cut correction has been applied. The raw numbers of collected events are given in parenthesis (no events with 4 charged detected tracks have been found).

Total C.M. energy $E_+ + E_-$ (GeV) (1)	Effective integrated luminosity (cm^{-2}) (2)	Corrected Bhabha events (3)	Non-coplanar events: 2τ events (4)	$2\tau + \gamma$ events (5)	$2\tau + 2\gamma$ events (6)	3τ events (7)	$3\tau + \gamma$ events (8)	Total non-coplanar events (9)
1.4	119×10^{32}	472±33	(55) 40.6± 9.4 (100)	(8) 6.4±3.5 (15)	(0) 0.0±1.1 (1)	(6) 5.4±2.5 (12)	(1) 0.6±1.1 (1)	(70) 53.0±10.4 (128)
1.5	231	720±34	90.7±12.1 (32)	11.1±4.8 (4)	1.0±1.2 (0)	11.1±3.8 (6)	0.6±1.5 (0)	114.5±13.7 (42)
1.6	67	166±17	26.5± 7.0 (44)	2.3±2.4 (7)	0.0±1.1 (2)	5.3±2.5 (2)	0.0±1.1 (2)	34.6± 7.9 (57)
1.65	76	170±17	28.2± 8.6 (59)	6.4±3.1 (7)	2.0±1.5 (1)	1.7±1.5 (1)	2.0±1.5 (0)	40.3± 9.5 (65)
1.7	130	261±21	42.9± 9.7 (46)	4.1±3.3 (4)	0.3±1.1 (0)	0.0±1.2 (4)	0.0±1.3 (0)	47.3±10.5 (54)
1.75	83	152±16	33.1± 8.5 (68)	1.8±2.8 (4)	0.0±1.1 (0)	3.4±2.1 (2)	0.0±1.2 (0)	38.3± 9.3 (74)
1.8	115	189±18	50.1±10.5 (110)	1.0±2.6 (23)	-0.3±1.1 (2)	2.0±1.5 (10)	-0.3±1.3 (2)	52.5±11.0 (146)
1.85	514	770±36	84.9±16.4 (45)	25.9±6.5 (3)	-2.0±1.7 (2)	10.6±4.2 (3)	2.7±2.3 (0)	122.1±18.6 (53)
1.9	122	166±17	24.5± 8.8 (145)	2.1±2.3 (7)	2.0±1.5 (0)	3.3±2.0 (5)	0.0±1.2 (0)	31.9± 9.5 (157)
2.0	257	293±25	90.4±17.9 (142)	5.8±3.7 (26)	0.0±1.1 (3)	5.8±2.7 (13)	-0.7±1.5 (2)	101.3±18.5 (184)
2.4	751	453±23	22.6±24.6	21.9±6.3	3.9±2.5	12.7±4.1	1.7±2.0	62.8±25.9
Totals	2465×10^{32}	3812±83	(846) 534.5±43.7	(108) 89.3±13.6	(11) 6.9±4.0	(64) 61.3±9.1	(8) 6.6±5.0	(1037) 698.6±47.1

the machine luminosity. This was done using the numbers of column (3) Table V. (The effective cross section to detect in our apparatus "4- and 3-chm" Bhabha events was computed by the M.C. program[24]). The effective luminosities calculated in this way are listed in column (2) of Table V.

The determination of the luminosity from the numbers of wide angle Bhabha events detected by our apparatus is particularly convenient in order to evaluate absolute values of the cross sections for the reactions $e^+e^- \rightarrow a^\pm + a^\pm$ + anything. In fact this procedure minimizes effects due to the uncertainty in the actual value of the source length[9] and in the spark chamber efficiency, which are in first approximation the same for the Bhabha and the non-coplanar events[25].

In conclusion we can summarize the results of Section V.1, V.2 and V.3 in the following way:

i) a total of 1037 non-coplanar events have been experimentally observed in a set of runs performed at machine energies ranging from $E_\pm = 0.7$ to $E_+ = 1.2$ GeV. The number of large angle Bhabha scattering events collected in our apparatus, in the same conditions was 3812, corresponding to an effective integrated luminosity $\sim 2.5 \cdot 10^{35}$ cm^{-2};

ii) after cosmic rays and machine background subtractions, 605 of the detected non-coplanar events appear to originate from e^+e^- interaction according to the reactions

$$e^+e^- \rightarrow a^\pm + b^\pm + \text{anything.} \qquad (V.1)$$

By applying the experimentally measured correction for the $\Delta\varphi$ cut to the non-coplanar events, the total number of events originated from reaction V.1 which are detected by our apparatus turns out to be 699;

iii) in addition to $a^\pm$ and $b^\pm$, sometimes additional charged and/or neutral particles are observed, demonstrating the existence of processes with at least 4 charged and 4 charged plus neutral particles produced;

iv) the produced particles are of hadronic nature with a very small possible contamination of electrons ($< 10\%$). Therefore in the following we will assume that all the emitted particles are pions, which is consistent with all of our experimental information.

V.4. - Analysis of the results, and absolute values of the cross-sections for the reaction $e^+e^- \rightarrow a^\pm + b^\pm$ + anything. -

The evaluation of cross sections from the experimental data requires the knowledge of the detection efficiency of our apparatus which, of course, depends on the states actually produced.

The yield (n_D) of events in each detected configuration D(D= 2τ, $2\tau + \gamma$, $2\tau + 2\gamma$, 3τ, etc.) is related to the cross-sections by the equation

$$n_D = \frac{N_D}{\mathcal{L}} = \sum_P \varepsilon_D^P \sigma_P \,. \qquad (V.3)$$

N_D are the total number of events detected in the configuration D; $\mathcal{L}$ is the integrated luminosity; σ_P is the cross-section to produce a definite channel P

(for example, P could be $e^+e^- \to \pi^+\pi^-\pi^0$, $e^+e^- \to \pi^+\pi^-\pi^+\pi^-$, etc.); and finally ε_D^P is the efficiency of our apparatus to detect the configuration D when the final particles are produced in channel P.

We have plotted in Fig. 16(a), (b) and (c) the experimental values of the yields for the detected configurations 2τ, $2\tau+\mathcal{N}$, 3τ which are the most statistically significant. We have grouped the data into three energy bins, centered at 1.51, 1.82 and 2.3 GeV (weighted average). In Fig. 16(d) the total yield summed over all the detected configurations is also shown for each $E_+ + E_-$ energy we have investigated.

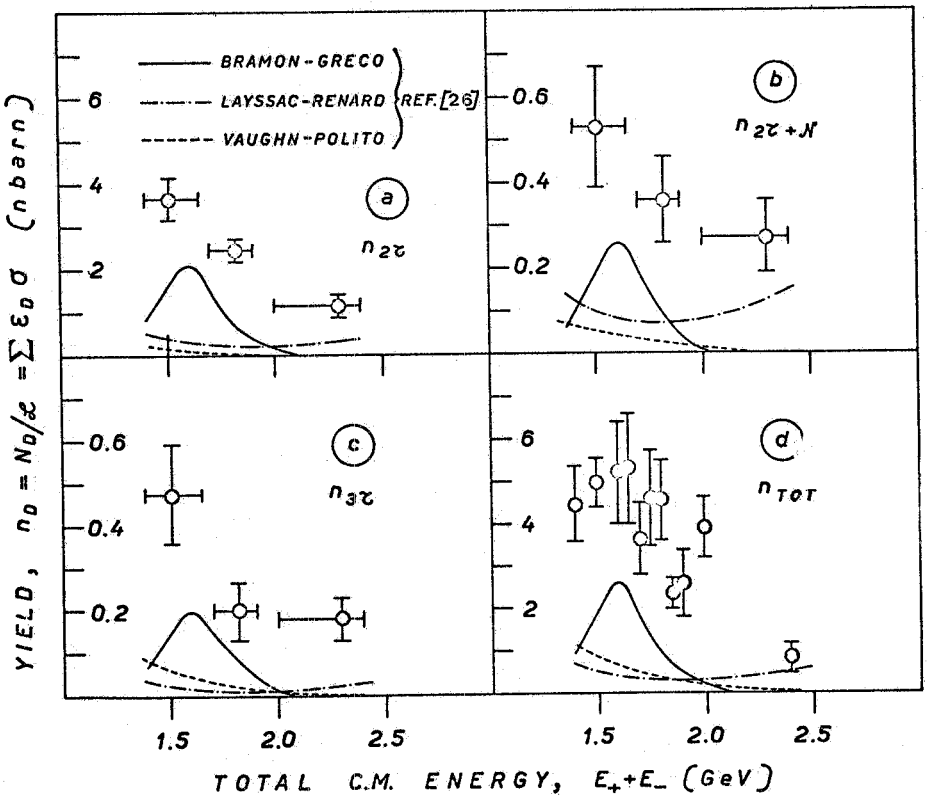

FIG. 16 - Yield of non-coplanar corrected events. a) Two charged tracks detected; b) two charged tracks plus one neutral detected; c) three charged tracks detected; d) total yield (all the detected configurations). The curves are predictions of some theoretical models.

Finally in Fig. 17 we show that the energy dependence of the yield is the same for each of the detected configurations.

By using equations (V.3) the prediction of any specific model, which provides the values of the σ_P's, can be easily compared with our n_D data, once the corresponding detection efficiencies ε_D^P have been calculated.

As an example, we have drawn in the same Fig. 16 the predictions of some theoretical models[26], using the efficiency values which are listed and

discussed in the Appendix A. - The agreement is unsatisfactory, since the theoretical predictions are much smaller than the experimental yields. The best prediction, in terms of absolute magnitude and energy dependence, is that of Bramon and Greco[26], based on the existence of a heavy vector meson ($J^P = 1^-, I=1$) ", whose parameters were deduced from the results of the SLAC streamer chamber group on the reaction $\gamma + p \rightarrow p\,\pi^+\pi^-\pi^+\pi^-$[27]. But even in this case our experimental yields are at least a factor of two larger than the prediction.

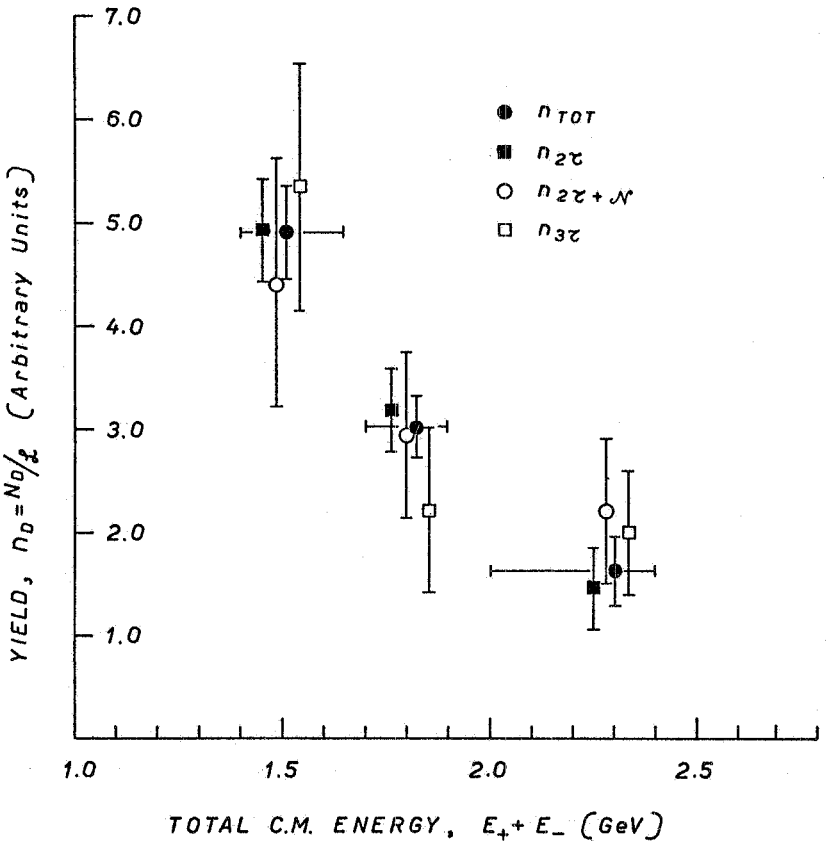

FIG. 17 - Energy dependence of the yields. Different configuration yields are normalized to the same area.

Conversely, instead of comparing the theoretical to the experimental yields, we can attempt to solve the set of equations (V.3) in terms of the unknown cross-sections σ_Ps. In fact, apart from the statistical significance of some our experimental numbers, we have in principle six different detected configurations (2τ, $2\tau+\mathcal{N}$, $2\tau+2\mathcal{N}$, 3τ, $3\tau+\mathcal{N}$, 4τ); i.e. six different equations (V.3). This would allow to extract from the data the cross-sections for six different channels P, once the detection efficiencies have been calculated.

Let us first make a few comments on the detection efficiencies ε_D^P. As it is discussed in Appendix A, for our experimental apparatus the calculated efficiencies turn out to be quite insensitive to the mechanism of production of each channel (at least in the most reasonable cases we have considered, namely: statistical and quasi-two body production). They have also quite similar values for an iso

tropic and a $\sin^2\theta$ production distribution. Therefore the values used in the analysis will be the ones we have calculated with the statistical model (invariant phase space (IPS) efficiencies). However, due to the small solid angle of the apparatus and the energy cuts on the detected particles, the values of the efficiencies are quite small, ranging from $\lesssim 1\%$ to $\sim 10\%$ depending on the produced channel and the detected configuration. Clearly this means that to obtain cross-sections we must multiply the observed number of events by a calculated, somewhat model dependent number, ranging from ~ 10 to more than 100 in the different cases. This results (in our opinion) in a strong limitation in the quality of the results which can be obtained on the cross-sections, with the existing small solid angle apparata.

Keeping in mind the above considerations, let us return to equations (V.3). Although this system of equations is not sufficient to be solved in all the possible σ'_Ps.(whose number is in principle limited only by energy conservation), some useful information about the σ'_Ps can be extracted, under reasonably weak hypothesis, from our data. We have proceeded as follows:

i) we complement the six eqs. (V.3) with an additional equation using the total number N_M of detected "marked" events (see section V.2 for reference). N_M is expressed in terms of the σ'_Ps by the following relation

$$N_M = \sum_P f_M^P \, \varepsilon^P \, \sigma_P \tag{IV.4}$$

The efficiencies $\varepsilon_P = \sum_D \varepsilon_P^D$ and the fractions of "marked" events due to the produced final state P, f_M^P, are known from the Montecarlo calculation (see Appendix A);

ii) we restrict the possible σ'_Ps to the following six physical channels:

$$\sigma_{2\pi^\pm\pi^o} = \sigma(e^+e^- \to \pi^+\pi^-\pi^o);$$

$$\sigma_{2\pi^\pm 2\pi^o} = \sigma(e^+e^- \to \pi^+\pi^- 2\pi^o);$$

$$\sigma_{4\pi^\pm} = \sigma(e^+e^- \to \pi^+\pi^-\pi^+\pi^-);$$

$$\sigma_{4\pi^\pm\pi^o} = \sigma(e^+e^- \to \pi^+\pi^-\pi^+\pi^-\pi^o);$$

$$\sigma_{4\pi^\pm 2\pi^o} = \sigma(e^+e^- \to \pi^+\pi^-\pi^+\pi^- 2\pi^o);$$

$$\sigma_{6\pi^\pm} = \sigma(e^+e^- \to \pi^+\pi^-\pi^+\pi^-\pi^+\pi^-)$$

Due to the numerical structure of eqs. (V.3) and (V.4), and to the statistical uncertainties, there is not an unique determination of all six chosen cross-sections. However, we have found that if we parametrize the best fit solutions as a function of

$$x = \frac{\sigma_{2\pi^\pm\pi^o} + \sigma_{2\pi^\pm 2\pi^o}}{\sigma_{4\pi^\pm} + \sigma_{4\pi^\pm\pi^o} + \sigma_{4\pi^\pm 2\pi^o} + \sigma_{6\pi^\pm}} = \frac{\sigma_{2\pi^\pm, N}}{\sigma_{\geq 4\pi^\pm, TOT}}$$

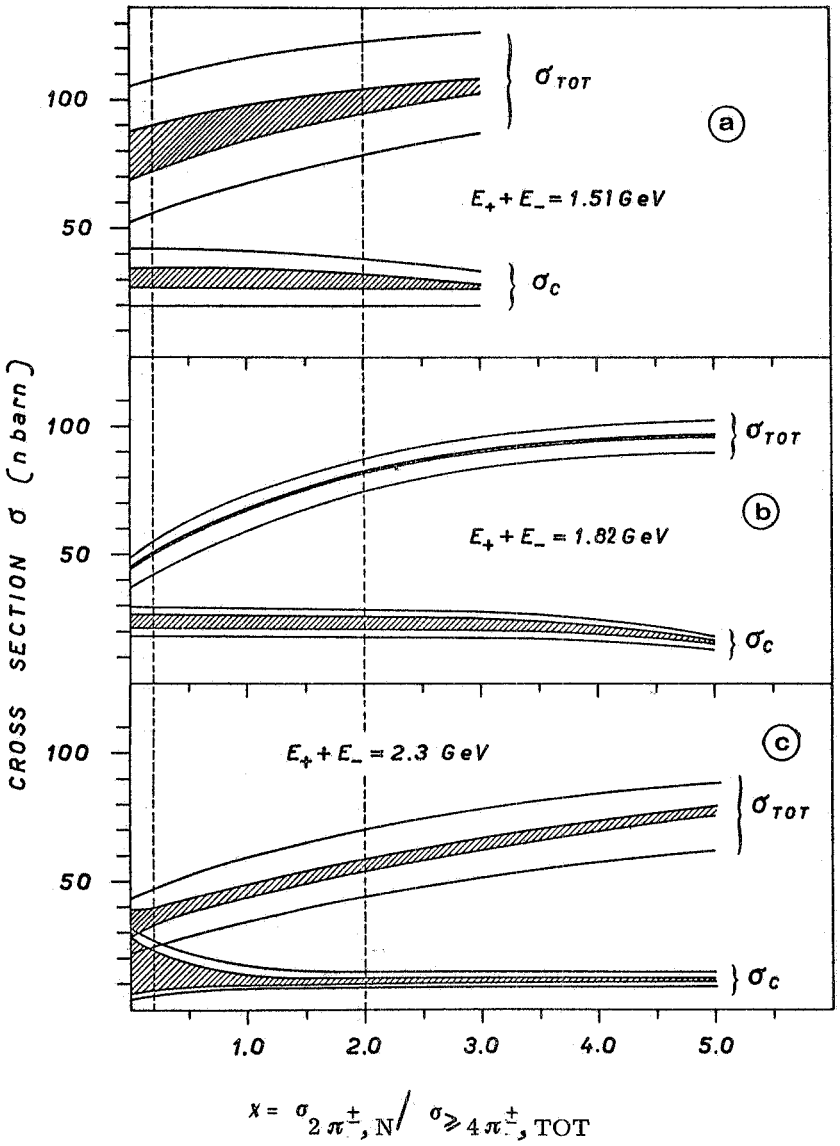

FIG. 18 - Reactions $e^+e^- \to a^\pm + b^\pm +$ anything: the total cross-section, σ_{TOT}, and $\sigma_C = \sigma_{4\pi^\pm} + \sigma_{6\pi^\pm}$ as a function of the parameter $x = (\sigma_{2\pi^\pm\pi^0} + \sigma_{2\pi^\pm 2\pi^0})/(\sigma_{4\pi^\pm} + \sigma_{4\pi^\pm\pi^0} + \sigma_{4\pi^\pm 2\pi^0} + \sigma_{6\pi^\pm})$. a) $\langle E_+ + E_- \rangle = 1.51$ GeV; b) $\langle E_+ + E_- \rangle = 1.82$ GeV; c) $\langle E_+ + E_- \rangle = 2.30$ GeV.

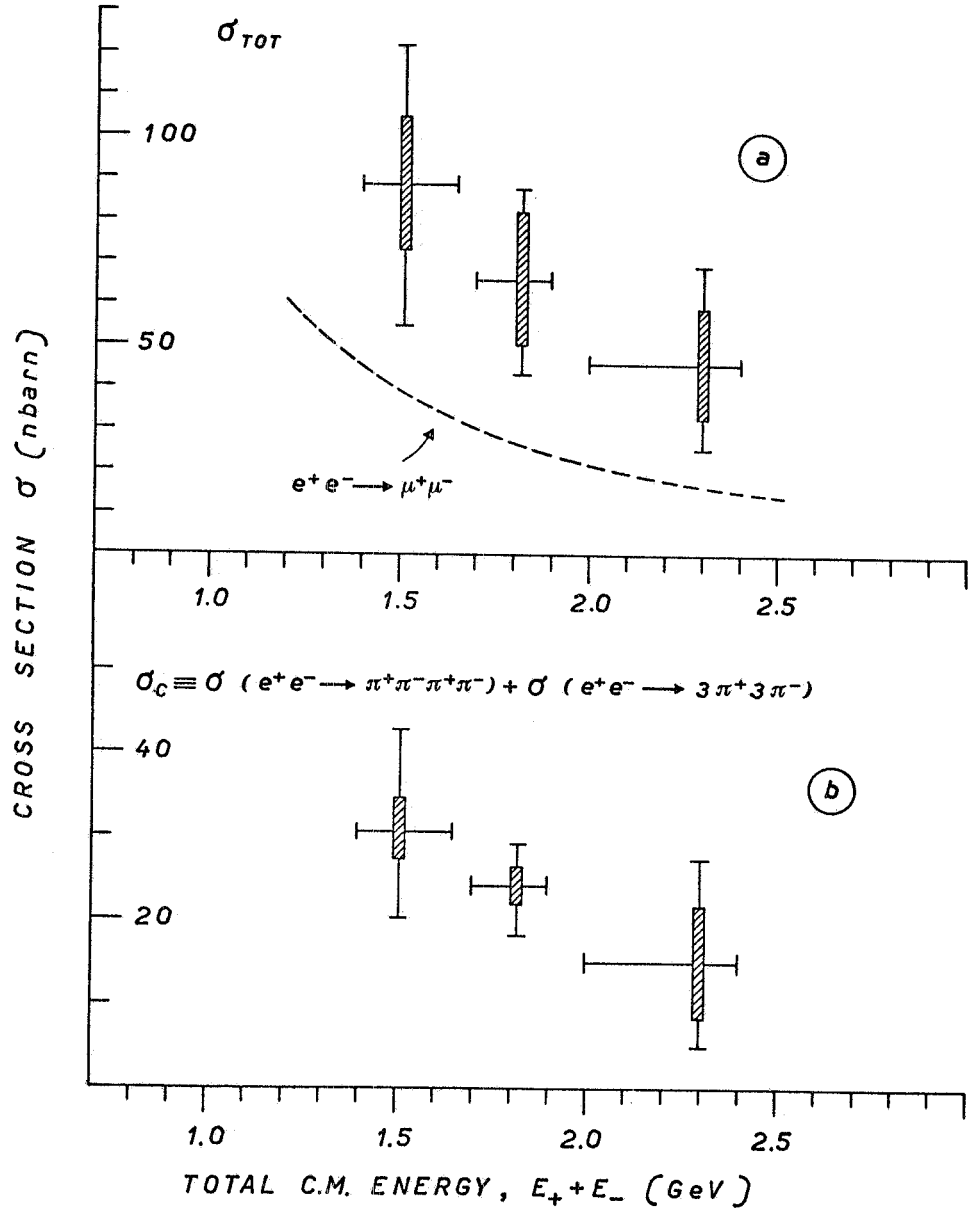

FIG. 19 - Reactions $e^+e^- \rightarrow a^{\pm} + b^{\pm}$ + anything: values of the cross sections for $0.2 \leq x \leq 2$. For each point the dashed rectangles indicate the range of values obtained as acceptable solutions of the fit, while the errors are shown as bars.
a) Total cross-section, σ_{TOT}; for reference, the total cross-section to produce a pair of μ mesons is also plotted; b) cross-section for totally charged produced particles, $\sigma_c = \sigma_{4\pi^{\pm}} + \sigma_{6\pi^{\pm}}$.

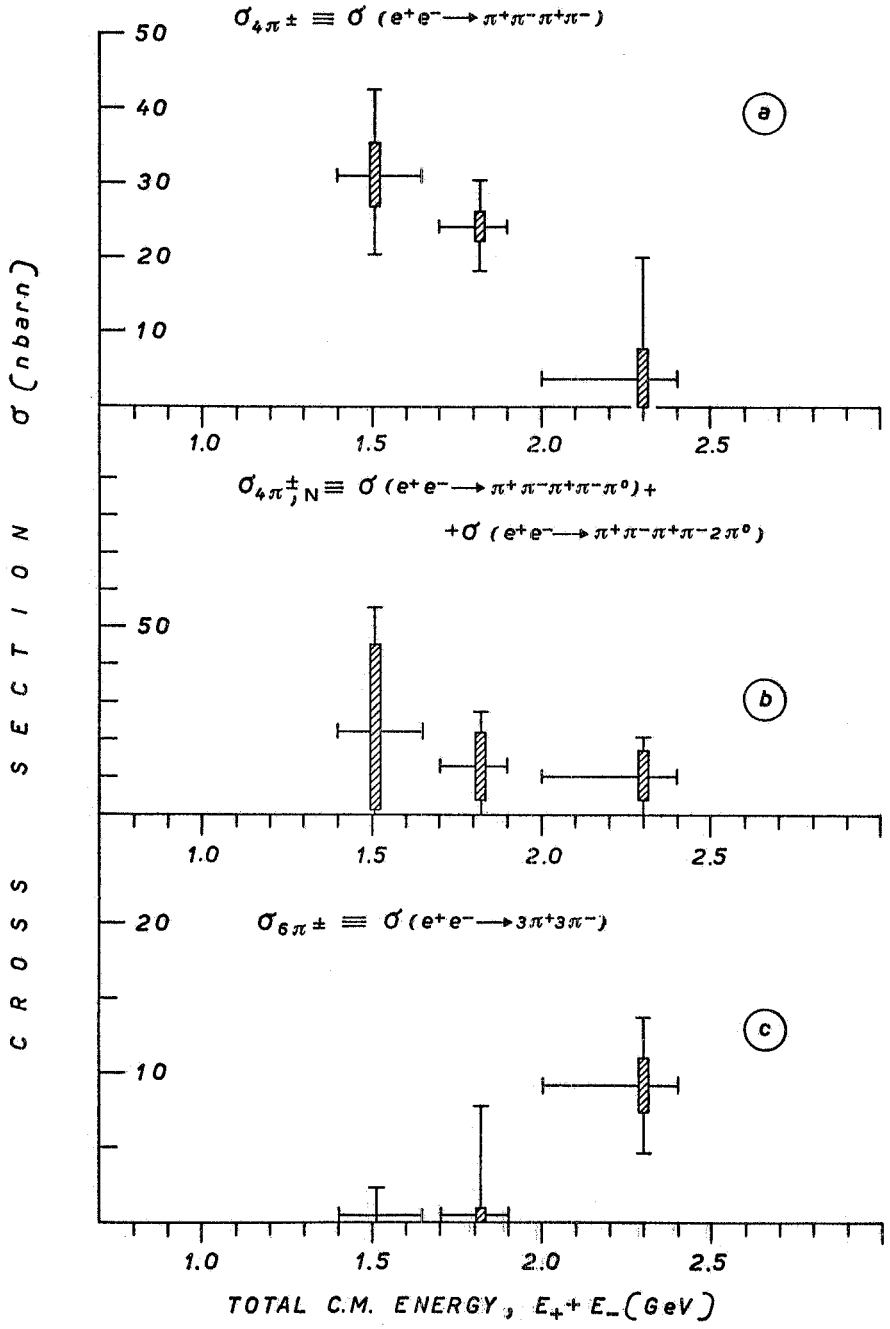

FIG. 20 - Reactions $e^+e^- \rightarrow a^{\pm} + b^{\pm}$ + anything: values of the cross-sections for $0.2 \lesssim x \lesssim 2$. For each point the dashed rectangles indicate the range of values obtained as acceptable solutions of the fit, while the errors are shown as bars. a) $\sigma_{4\pi^{\pm}}$; b) cross-section to produce 4 charged particles plus neutrals, $\sigma_{4\pi^{\pm},N}$; c) $\sigma_{6\pi^{\pm}}$.

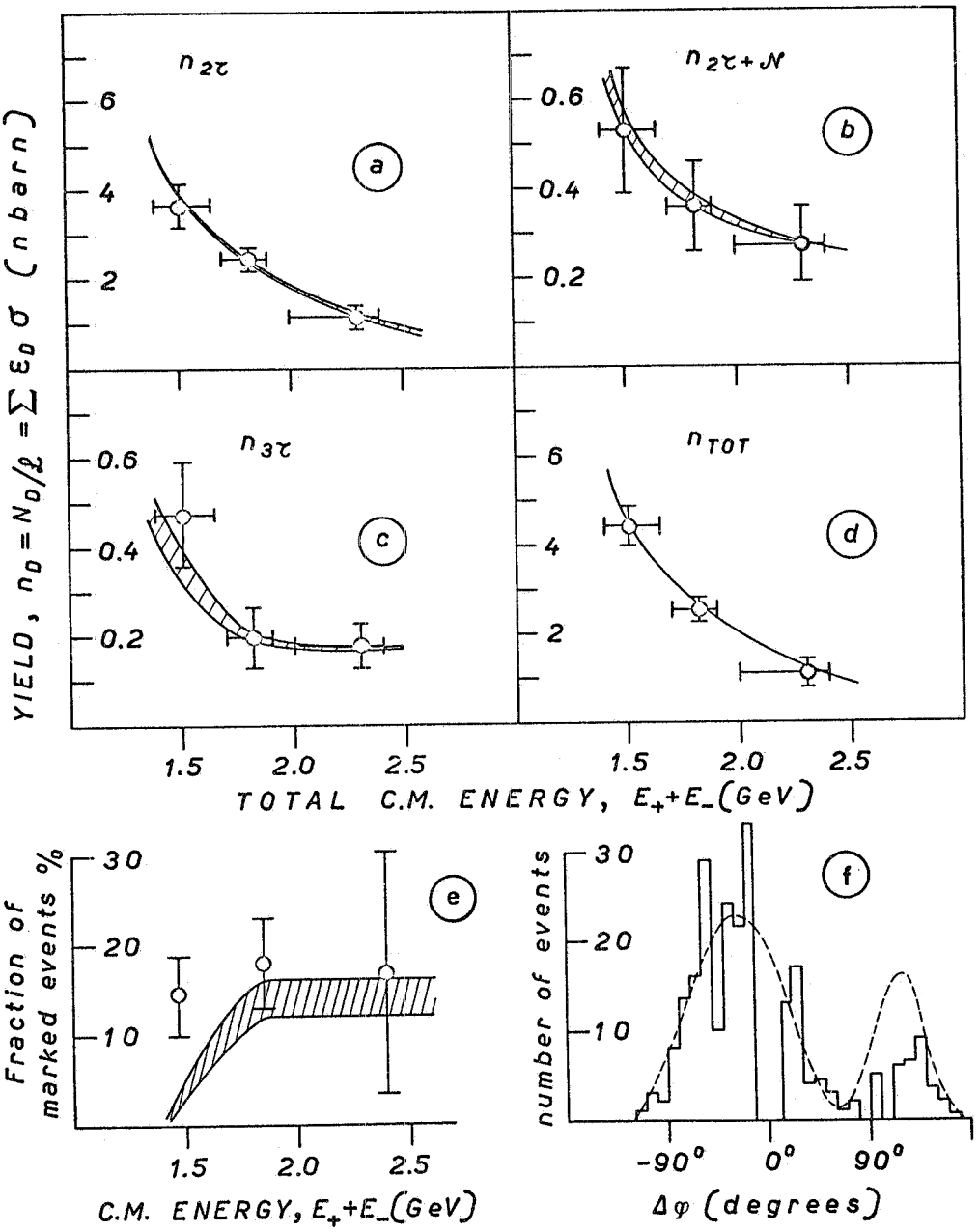

FIG. 21 - Comparison of the experimental data on the reactions $e^+e^- \rightarrow a^{\pm} + b^{\mp}$ + anything with the results of the fit (shown as curves and dashed bands in the Figure). a) Yield of two charged detected tracks events; b) yield of two charged plus one neutral detected tracks events; c) yield of three charged detected tracks events; d) total yield (all the detected configurations); e) fraction of "marked" events; f) $\Delta\varphi$ distribution ("4-chm" events).

in all the different energy intervals explored there is a class of solutions with acceptable χ^2. In fact at all three considered averaged energies there is a clear separation between a set of accectable solutions, for which the values of χ^2 are clustered together, and the rejected solutions corresponding to higher χ^2 values[28]. Moreover it turned out that some particular combinations of the σ_P's are rather well determined: expecially the total cross-section $\sigma_{TOT} = \sigma_{2\pi^\pm\pi^0} + \sigma_{2\pi+2\pi^0} + \sigma_{4\pi^+} + \sigma_{4\pi^\pm\pi^0} + \sigma_{4\pi^\pm+2\pi^0} + \sigma_{6\pi^\pm}$ and the cross section for totally charged produced particles $\sigma_C = \sigma_{4\pi^\pm} + \sigma_{6\pi^\pm}$. In addition, with somewhat larger uncertainty, we can also determine $\sigma_{4\pi^\pm}$ and $\sigma_{6\pi^\pm}$ separately, as well as $\sigma_{4\pi^\pm, N} = \sigma_{4\pi^\pm\pi^0} + \sigma_{4\pi^\pm 2\pi^0}$.

Fig. 18 shows the parametrization of σ_{TOT} and σ_C with respect to x, for each of the three average energies. There were no acceptable solutions for values of the parameter $x \geqslant 3$ at 1.51 GeV, and $x \geqslant 5$ at 1.82 and 2.3 GeV C.M. energies. For all the class of acceptable solution, the values obtained for σ_{TOT} and σ_C fall in the region, indicated by the dashed bands, with statistical errors indicated by the white band.

If we restrict the value of x to the region $0.2 \leqslant x \leqslant 2$, then σ_{TOT} and σ_C are determined as shown in Figs. 19(a) and (b). With the same criteria also $\sigma_{4\pi^\pm}$, $\sigma_{4\pi^\pm, N}$ and $\sigma_{6\pi^\pm}$ are determined, with somewhat larger error, as shown in Figs. 20(a), (b) and (c). The interval of x chosen is conservatively large. In fact the ratio $\sigma_{2\pi^\pm, N} / \sigma_{\geqslant 4\pi^\pm, TOT}$ is always $\geqslant 0.2$ for any possible isotopic spin configuration, thus setting the lower limit for x. On the other hand, a value of x larger than 2 is strongly inconsistent with the results of all the other Adone groups[30].

Finally in Fig. 21 we compare our experimental data (i.e. the yields for each different detected configuration, the fraction of marked events and the $\Delta\varphi$ distribution) with the results obtained, using the admixture of final states indicated by the best fit procedure, from the invariant phase space (IPS) Montecarlo program (see Appendix A). The general agreement is quite satisfactory, the only discrepant experimental point being the fraction of "marked" events at 1.51 GeV which we have already discussed in Ref. (28).

V.5. - Conclusions. -

We can summarize the experimental information on the reaction $e^+e^- \longrightarrow a^\pm + b^\pm +$ anything as follows:

a) we have collected 605 events originated from the above reaction, at C.M. energies between 1.4 and 2.4 GeV, for a total integrated luminosity $\mathcal{L} \simeq \simeq 2.5\, 10^{35} cm^{-2}$;

b) on the basis of pulse height distribution and absorption properties, $a^\pm$ and $b^\pm$ appear to be hadrons, the possible contamination from electrons being demonstrated to be less than $\sim 10\%$;

c) the total possible contamination from reactions of the type $e^+e^- \rightarrow e^+ + e^- +$ anything via a two-photon-interaction channel[22, 23] is negligible ($<10\%$) in the non-coplanarity region investigated ($|\Delta\varphi| \geqslant 13^\circ$);

d) the experimental yield appears to be much larger than is predicted on the basis of the ϱ, ω and φ dominance at these energies;

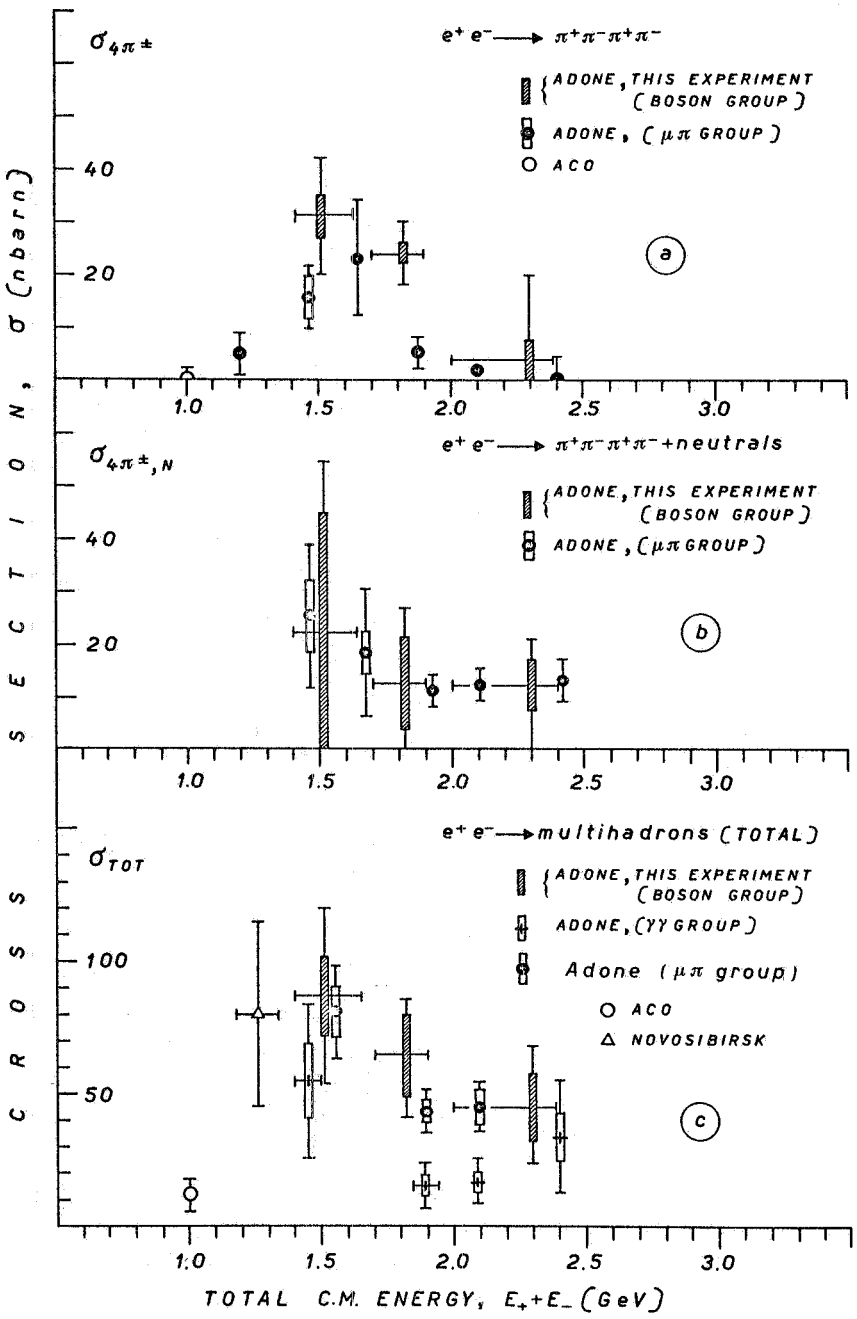

FIG. 22 - Summary of the experimental determinations of the cross-sections for reactions $e^+e^- \rightarrow a^{\pm} + b^{\pm}$ + anything. Our result are compared with the data from ACO (Ref. (31a)), Novosibirsk (Ref. (31b)), Adone $\gamma\gamma$ group (Ref. (31c)) and Adone $\mu\pi$ group (Ref. (31d)). a) $\sigma_{4\pi^{\pm}}$; b) cross-section to produce 4 charged pions plus neutrals, $\sigma_{4\pi^{\pm},N}$; c) total cross-section, σ_{TOT}.

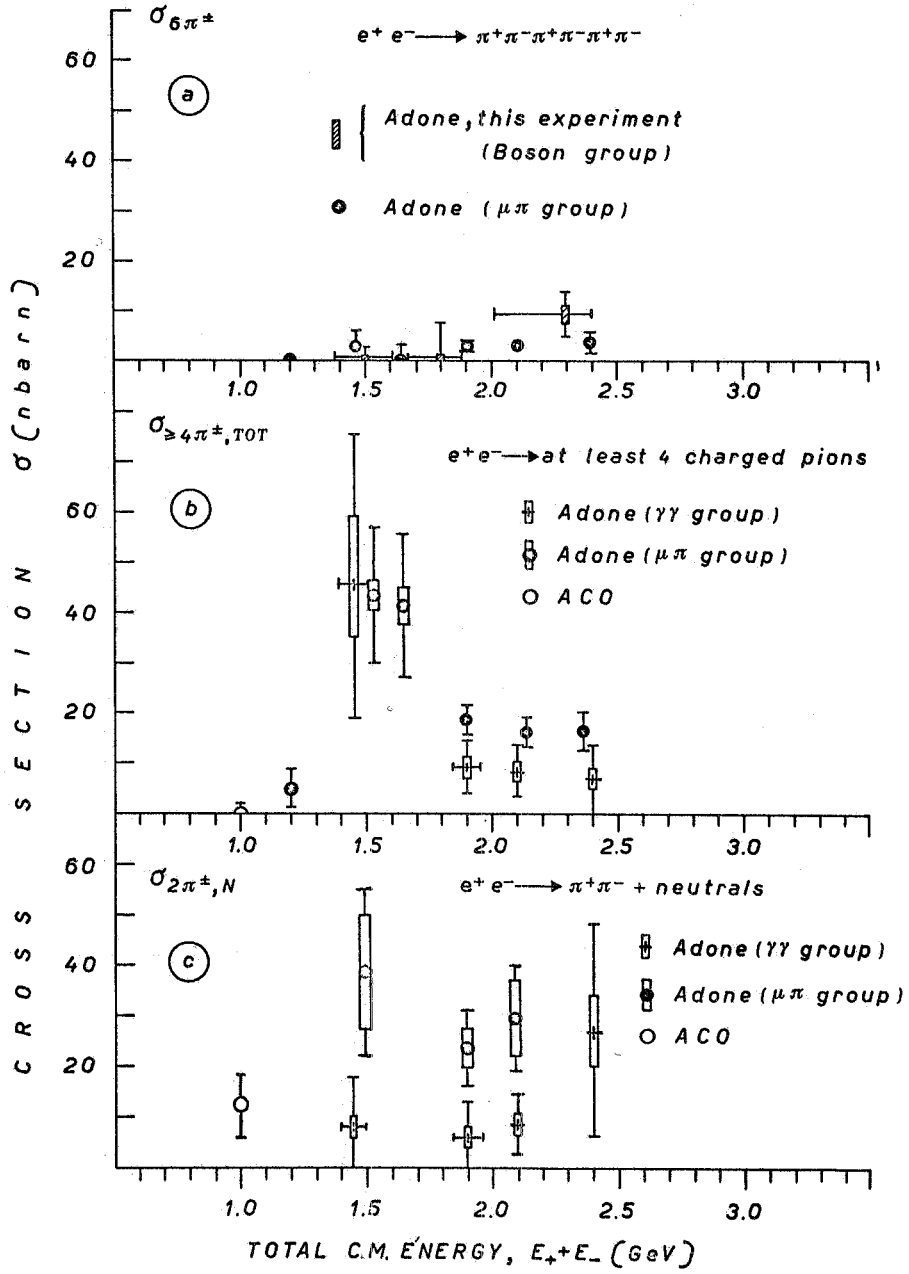

FIG. 23 - Summary of the experimental determinations of the cross-sections for reactions $e^+e^- \rightarrow a^\pm + b^\pm +$ anything. Our results are compared with the data from ACO (Ref. (31a)), Adone $\gamma\gamma$ group (Ref. 31c)) and Adone $\mu\pi$ group (Ref. (31d)). a) $\sigma_{6\pi^\pm}$; b) cross-sections to produce at least 4 charged pions (plus possible neutrals), $\sigma_{\geq 4\pi^\pm, TOT}$; c) cross-sections to produce 2 charged pions plus neutrals, $\sigma_{2\pi^\pm, N}$.

e) the total cross section for reaction $e^+e^- \rightarrow a^{\pm} + b^{\pm}$ + anything has been determined. The obtained values, turn out to be surprisingly larger than one would have expected, ranging from 50 to 90 nbarns, in the energy interval 1.4 to 2.4 GeV. In Fig. 22(c) our results are compared with those of other experiments[31, a, b, c, d]. There appears to be rather striking increase of the cross section between 1 and 1.5 GeV, followed by a slow fall-off consistent with a $1/s$ dependence.

f) The cross sections for some particular final states have also been determined. A summary of all the experimental information from this and the other experiments[31, a, b, c, d] is given in Figs. 22 and 23. The energy behaviour does not appear to be the same in the different channels. A resonant behaviour could possibly explain the $e^+ + e^- \rightarrow \pi^+\pi^-\pi^+\pi^-$ channel as discussed in reference[31d].

ACKNOWLEDGEMENTS. -

We wish to thank the many people who worked in the early stages of this experiment: B. Coluzzi, G. Goggi, F. Massa, P. Scannicchio and N. Spinelli, and in particular C. Bernardini for having stimulated this experiment and for continuous encouragement and useful discussion. Our technician Gianni Schina made a valuable contribution to the setting up and maintenance of the apparatus. The monitor group made available to us their luminosity measurements. Finally we thank the Adone staff for their co-operation, Dr. A. Rambaldi for considerable assistence in the computer analysis, and all the members of the other A done groups for continuous discussion.

APPENDIX A. - THE MONTECARLO CALCULATION. -

In order to understand the response of our experimental apparatus to the reactions which were the object of our experimental study (i.e. elastic electron-positron scattering and production of multihadron states) we have performed a Montecarlo (MC) calculation. This calculation takes into account, in addition to the geometrical features of the apparatus, also the energy cuts (range), the nuclear absorption (see Appendix B), the efficiency of the spark chambers, and the effects of the extended source (see Ref. (9), Section II). For the elastic electron-positron scattering we have made use of the Bhabha cross-section. For the multihadron processes several different models have been used. We report in this appendix the results which are of interest for the interpretation of our data.

First, in Table A.I we list, at three different C.M. energies, the values of the detection efficiencies which were used for the analysis of our experimental data. They refer to the processes

$$e^+e^- \rightarrow n\pi^+ + n\pi^- + m\pi^o$$

Angular and energy distributions have been calculated in the frame of the statistical model (invariant phase space, IPS, distributions). To give a quantitative feeling of how much the different effects involved affect the values of the efficiencies, we refer, as a typical example, to the efficiency $\varepsilon_{2\tau}^{4\pi^\pm}$ to detect a two-charged configuration (2τ) from the reaction $e^+e^- \rightarrow \pi^+\pi^-\pi^+\pi^-$, calculated at total C.M. energy $E_+ + E_- = 1.8$ GeV. Taking into account only the geometry of the apparatus, for a point-like source ε would be $\sim 29\%$. The effect of the extended source is to lower ε to $\sim 14.5\%$. Including the low energy cut (determined by the amount of absorber before the trigger counters in our telescopes) ε becomes 13%, and $\varepsilon = 8\%$ when the upper energy cut (due to the CR veto counters) is taken into account. Switching-on nuclear interactions brings ε to $\sim 9\%$, and finally the spark chamber inefficiency reduces ε to 7%. The relatively small effect of the nuclear interactions (which appear to produce a net variation of $\sim 10\%$ in the value of the efficiency) is the result of a partial cancellation: in fact while nuclear interactions increase the importance of the absorbers between the trigger counters in the telescopes, at the same time they reduce from 40% to $\sim 10\%$ the fraction of events in which a particle, crossing the iron roof absorber is vetoed by the CR counters. Finally, it is interesting to recall (see Section V.3) that we have used the rate of the wide angle e^+e^- elastic scattering events collected in our apparatus as a luminosity monitor for the hadronic events. The fact that we have computed the detection efficiency for e^+e^- pair with the same Montecarlo minimizes the effects on the cross-sections of uncertainties in the actual values of the source lenght and of the spark efficiencies of the wire chambers.

In Table A.II we give instead the values of the detection efficiencies for 4 pion final states, calculated with different dynamical models, via quasi two-body intermediate states, namely:

$$e^+e^- \rightarrow A_1^\pm \pi^\mp \rightarrow \pi^+\pi^-\pi^o\pi^o \text{ or } \pi^+\pi^-\pi^+\pi^-, \qquad e^+e^- \rightarrow A_2^\pm \pi^\mp \rightarrow \pi^+\pi^-\pi^o\pi^o \text{ or } \pi^+\pi^-\pi^+\pi^-$$

$$e^+e^- \rightarrow \omega\pi^o \rightarrow \pi^+\pi^-\pi^o\pi^o$$

TABLE A.I

Values of the statistical efficiencies to detect in our apparatus any particular experimental configuration, for several possible produced final states of pions, at three different values of the total C.M. energy, $E_+ + E_-$. Invariant phase space distribution of the produced particles was assumed.

Produced final state	$E_+ + E_-$ (GeV)	Efficiency for detection of 2τ (%)	$2\tau + 1\mathcal{N}$ (%)	$2\tau + 2\mathcal{N}$ (%)	3τ (%)	$3\tau + 1\mathcal{N}$ (%)	4τ (%)
$\pi^+ \pi^- \pi^o$	1.4	2.2	0.7	0.0			
	1.8	1.4	0.5	0.0			
	2.4	0.6	0.2	0.0			
$\pi^+ \pi^- 2\pi^o$	1.4	1.1	0.7	0.2			
	1.8	1.0	0.7	0.1			
	2.4	0.7	0.4	0.1			
$\pi^+ \pi^- 3\pi^o$	1.4	0.5	0.4	0.2			
	1.8	0.6	0.5	0.2			
	2.4	0.6	0.3	0.2			
$\pi^+ \pi^- 4\pi^o$	1.4	0.1	0.2	0.1			
	1.8	0.2	0.4	0.2			
	2.4	0.2	0.3	0.2			
$\pi^+ \pi^- \pi^+ \pi^-$	1.4	8.5			0.9		0.0
	1.8	7.0			0.7		0.0
	2.4	4.0			0.4		0.0
$\pi^+ \pi^- \pi^+ \pi^- \pi^o$	1.4	4.0	1.5	0.0	0.4	0.1	0.0
	1.8	4.1	1.4	0.0	0.4	0.1	0.0
	2.4	3.5	1.0	0.0	0.2	0.1	0.0
$\pi^+ \pi^- \pi^+ \pi^- 2\pi^o$	1.4	1.6	1.0	0.1	0.1	0.1	0.0
	1.8	2.4	1.7	0.4	0.3	0.1	0.0
	2.4	2.0	1.4	0.3	0.2	0.2	0.0
$3\pi^- 3\pi^+$	1.4	6.5			0.6		0.0
	1.8	8.8			1.3		0.1
	2.4	7.4			1.1		0.1
$4\pi^+ 4\pi^-$	1.4	0.1			0.0		0.0
	1.8	6.3			0.7		0.0
	2.4	8.3			1.8		0.1

TABLE A.II

Values of the efficiencies to detect in our apparatus any particular experimental configuration from 4 pions final states, produced via a quasi-two-body intermediate state.

Produced final state	$E_+ + E_-$ (GeV)	Efficiency for detection of 2τ (%)	$2\tau + 1\mathcal{N}$ (%)	$2\tau + 2\mathcal{N}$ (%)	3τ (%)	$3\tau + 1\mathcal{N}$ (%)	4τ (%)
$\omega\,\pi^0$ ↓ $\pi^+\pi^-2\pi^0$	1.4	0.5	0.4	0.1			
	1.8	0.4	0.2	0.0			
	2.4	0.3	0.2	0.1			
$A_1^{\pm}\,\pi^{\mp}$ ↓ $\pi^+\pi^-2\pi^0$	1.4	1.0	0.6	0.2			
	1.8	1.1	0.7	0.1			
	2.4	0.6	0.4	0.0			
$A_2^{\pm}\,\pi^{\mp}$ ↓ $\pi^+\pi^-2\pi^0$	1.4	0.4	0.3	0.1			
	1.8	1.0	0.5	0.1			
	2.4	0.5	0.4	0.1			
$A_1^{\pm}\,\pi^{\mp}$ ↓ $\pi^+\pi^-\pi^+\pi^-$	1.4	8.9			0.9		0.0
	1.8	7.3			0.6		0.0
	2.4	3.6			0.4		0.0
$A_2^{\pm}\,\pi^{\mp}$ ↓ $\pi^+\pi^-\pi^+\pi^-$	1.4	7.7			0.6		0.0
	1.8	7.3			0.6		0.1
	2.4	4.1			0.5		0.0

The intermediate particles (A_1, A_2, ω) have been assumed to decay isotropically and to be statistically produced. We have checked that a production distribution of the type $A + B \sin^2\theta$, because of the extension of the source does not appreciably affect the values of the efficiencies (few % variations), irrespective of the values chosen for A and B. It can be seen from Table A.II that the efficiencies for these quasi two body channels do not differ, apart from threshold effects, from the corresponding statistical efficiencies (Table A.I) by more than 10-20%; the only exception being the case $e^+e^- \to \omega\pi^0$, whose detection efficiency is twice as small as for the corresponding statistical channel $e^+e^- \to \pi^+\pi^-\pi^0\pi^0$. It is worthwhile to note that the values of cross-sections obtained from our experimental data, using the efficiencies of either Tables A.I or A.II, turn out to be the same within the statistical errors.

In Figs. A.1 we show, as a function of the C.M. energy, the fraction, f_M, of events which, according to the MC calculation, are expected to be "marked". For reference, we have also plotted in the same figure the experimental values of f_M (see Section V.2).

Finally, in Fig. A.2 the $\Delta\varphi$ distributions calculated with the MC program for several different channels are shown. Fig. A.2(a) refers to $E_+ + E_- = 1.5$ GeV while Figs. A.2(b) and (c) refer to 1.8 and 2.3 GeV respectively. Apart from the $e^+e^- \to \omega\pi^0$ and $e^+e^- \to \pi^+\pi^-\pi^0$ (IPS) channels, which show a peculiar behaviour, the $\Delta\varphi$ distributions of all the other channels can be grouped in the two different typical distribution shown in Fig. A.2.

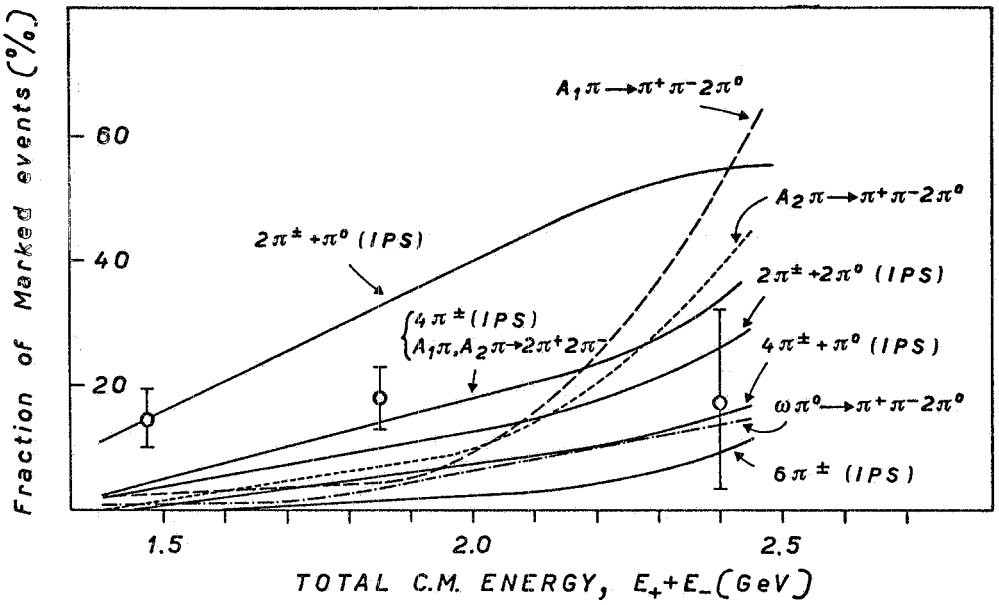

FIG. A. 1. - Fraction of "marked" events, f_M, calculated with the Montecarlo program for several different processes, compared with the experimental values.

APPENDIX B. - ABSORPTION AND SECONDARY PARTICLE PRODUCTION CALCULATION. -

B.1. - Absorption. -

We wish to calculate the fraction of primary pions that remains in a beam of pions after passing through a series of consecutive absorbers, consisting of different materials. Table B.I lists the constituents of one of the telescopes of our experimental apparatus.

If N_o is the initial number of pions, then

$$N_{1,pr} = N_o \, e^{-x_1/\lambda_{1,abs}}$$

is the number of π's remaining after the first absorber, x_1 is the path length and $\lambda_{1,abs}$ is the absorption length. Clearly the expression for the number ($N_{tot,pr}$) of pions remaining after a series of n absorbers, is

$$N_{tot,pr} = N_o \, e^{-\sum_{i=1}^{n} x_i/\lambda_{i,abs}} \qquad \text{(B.1)}$$

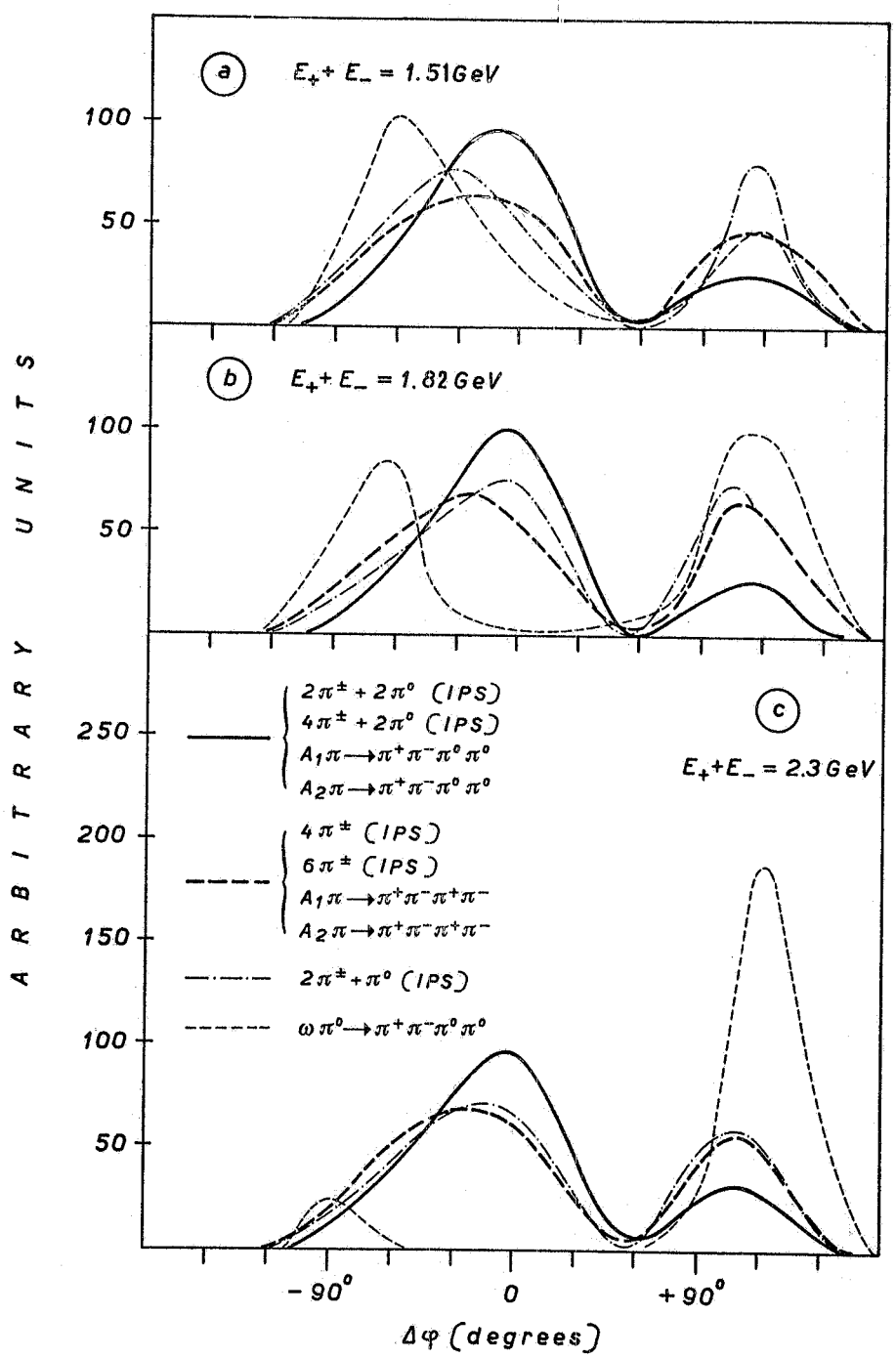

FIG. A.2 - $\Delta\varphi$ distribution calculated with the Montecarlo program for several different processes. a) $E_+ + E_- = 1.5$ GeV; b) $E_+ + E_- = 1.8$ GeV; c) $E_+ + E_- = 2.3$ GeV.

TABLE B.1

List of materials and corresponding thicknesses of one of the top telescopes (the bottom telescopes end after counter D_i).

Material	Thickness (g/cm^2)
Fe (vacuum chamber walls)	1.2
Glass (wire chamber SC α_i)	1.1
Scintillator (counter A_i)	2.0
Al	5.2
Scintillator (counter B_i)	1.4
Al	1.7
Glass (wire chamber SC β_i)	1.1
Pb	8.0
Fe	1.6
Scintillator (counter C_i)	2.8
Fe	1.6
Pb	8.0
Fe	1.6
Scintillator (counter D_i)	2.8
Fe	1.6
Al	2.4
Fe (22 cm)	158.0
Cardboard	0.5
Scintillator (counter CR_1 (CR_2))	2.2
Cardboard	0.5
Fe (1.5 cm)	19.0
Pb (5 cm)	56.7
Cardboard	0.5
Scintillator (counter CR_3 (CR_4))	2.2

B.2.- Secondary particle production.-

To begin this calculation of secondary particle production we must first define σ_{abs} (λ_{abs}) as the cross-section (the absorption length) for the particle to have any inelastic interaction, independent of the number of secondaries produced. So we write the probability (P) to produce a secondary with a certain minimum energy E_m between x and x+dx in an absorber of thickness T as

$$P(x,\theta)\,dx = e^{-x/\lambda_{abs}} \frac{dx}{\lambda_{abs}} \; p(\theta, E_m)$$

where $e^{-x/\lambda_{abs}}$ is the fraction of pions remaining at the point x, dx/λ_{abs} is the probability of interaction in dx, and $p(\theta, E_m)$ is the probability to produce a secondary (once a pion has been absorbed) within a specific angle θ (for istance the

aperture of the solid angle subtended by a counter placed after the absorber T), with a certain minimum energy E_m (for instance, the minimum energy necessary to emerge from T). Moreover the probability (P_s) that the secondary pions remain (are not absorbed) after they pass through the remaining (T-x) absorber is

$$P_s(x) \simeq e^{-(T-x)/\lambda_{abs}}$$

So, integrating through the whole absorber we can write for the number N_{sec} of secondary particles emerging from the absorber T:

$$N_{sec} = N_o e^{-T/\lambda_{abs}} \frac{T}{\lambda_{abs}} \overline{p(\theta, E_m)} \tag{B.2}$$

N_o is the number of incident pions and $\overline{p(\theta, E_m)}$ is the average of $p(\theta, E_m)$ over the whole absorber T.

The total number (N_{tot}) of pions emerging from the absorber T, will be then given by:

$$N_{tot} = N_{pr} + N_{sec} = N_o e^{-T/\lambda_{abs}} + N_o e^{-T/\lambda_{abs}} \frac{T}{\lambda_{abs}} \overline{p(\theta, E_m)} =$$

$$= N_o e^{-T/\lambda_{abs}} \left(1 + \frac{T}{\lambda_{abs}} \overline{p(\theta, E_m)}\right) \tag{B.3}$$

We can now proceed with the calculation for n absorbers by noticing that (for instance) the number of secondaries that are produced in the second absorber (of thickness x_2) and appear after the n^{th} absorber is

$$N_{2,sec} = (N_o e^{-x_1/\lambda_{1,abs}}) e^{-x_2/\lambda_{2,abs}} \frac{x_2}{\lambda_{2,abs}} \overline{p'_2(\theta_2, E_{2,m})} \left(e^{-\sum_{i=3}^{n} x_i/\lambda_{i,abs}}\right)$$

So, summing from all n absorbers, we have

$$N_{tot,sec} = N_o \sum_{i=1}^{n} \frac{x_i \overline{p'_i(\theta_i, E_{i,m})}}{\lambda_{i,abs}} \left[e^{-\sum_{i=1}^{n} x_i/\lambda_{i,abs}}\right] \tag{B.4}$$

By summing Eqs. (B.1) and (B.4), the total number (N_{tot}) of pions remaining after the set of n absorbers is given by:

$$N_{tot} = N_{tot,pr} + N_{tot,sec} = N_o e^{-\sum_{i=1}^{n} x_i/\lambda_{i,abs}} \left[1 + \sum_{i=1}^{n} \frac{x_i \overline{p_i(\theta_i, E_{i,m})}}{\lambda_{i,abs}}\right] \tag{B.5}$$

B.3.- Measurements of absorption cross-section and secondary particle production cross-section.-

Experimental determination of σ_{abs} and σ_{sec} have been measured by several groups[32-36]. In general, we have made use only of those counter experiment data that conform mostly to our experimental set up.

Measurements[32, 33] have determined the absorption cross-section (σ_{abs}) by fitting the experimental results assuming that:

$$\sigma_{exp} = \sigma_{diff} + \sigma_{abs} - \sigma_{sec} \cdot \tag{B.6}$$

σ_{sec} (the secondary particle production cross-section) was assumed to have an isotropic angular distribution, and σ_{diff} (the elastic scattering cross-section) was calculated using an optical model. For each of the References (32-36) the values of σ_{abs} determined for different elements from the experiments are shown in Fig. B.1 as a function of the pion kinetic energy, E_π. These values of σ_{abs} have been divided by $\sigma_{geom} = A^{2/3} (\hbar/m_\pi c)^2$. The graph indicates that within the errors at each energy the ratio of the absorption to geometrical cross-section is the same for all elements. This allows one to write a single energy dependence of $\sigma_{abs}/\sigma_{geom}$ for all elements. The energy dependence shows the effect of the (3,3) resonance near $E_\pi = 200$ MeV, but is almost constant ($\sigma_{abs}/\sigma_{geom} \sim 0.7$) at higher energies (consistently with the usual convention $\sigma_{abs} \simeq (2/3)\, \sigma_{geom}$). We define for further use $R(E_\pi) = \sigma_{abs}(E_\pi)/\sigma_{geom}$.

From Refs. (32, 33, 36), the Figs. B.2(a) and (b) show the energy and A dependence of σ_{sec} determined from fits to σ_{exp}. (For the secondary particle cross-section a form $\sigma_{sec} = 2\pi\eta(1-\cos\theta)$ was assumed, that is a isotropic production of secondaries). As it can be seen, secondary particle production is quite small below 200 MeV but rises linearly with pion incident energy. By using the curves in Fig. B.2(a) and (b) η (and therefore σ_{sec} for any solid angle $\Delta\Omega(\theta, \varphi)$) can be determined.

In addition, measurements of the energy distributions of secondaries has been carried out by several experiments[36]. Fig. B.3 shows the results of these measurements plotted in a useful manner. For each secondary percentage energy loss (F_E) the fraction of secondaries with an energy loss less than F_E have been plotted. That is, for any cut on the energy (expressed as a fraction of the incident pion energy) the graph indicates directly the percentage of the secondaries that survive this cut. The dashed line in Fig. B.3 is an average used in the calculation. All of these experimental determinations assume that the total number of pions emerging from an absorber of thickness T is given by

$$N_{tot} = N_o\, e^{-T/\lambda_{abs}}\, e^{T\,\sigma_{sec}\mathcal{N}_A/A} \tag{B.7}$$

where: $\sigma_{sec} = 2\pi\eta(1-\cos\theta)$; $\mathcal{N}_A$ is the Avogadro's number and A is the atomic weight of the absorber. By comparing Eq. (B.7) with Eq. (B.3), we can make the following identification with our previous notations:

$$\frac{T}{\lambda_{abs}} \quad \overline{p(\theta, E_m)} \Rightarrow \frac{T\,\sigma_{sec}\mathcal{N}_A}{A}$$

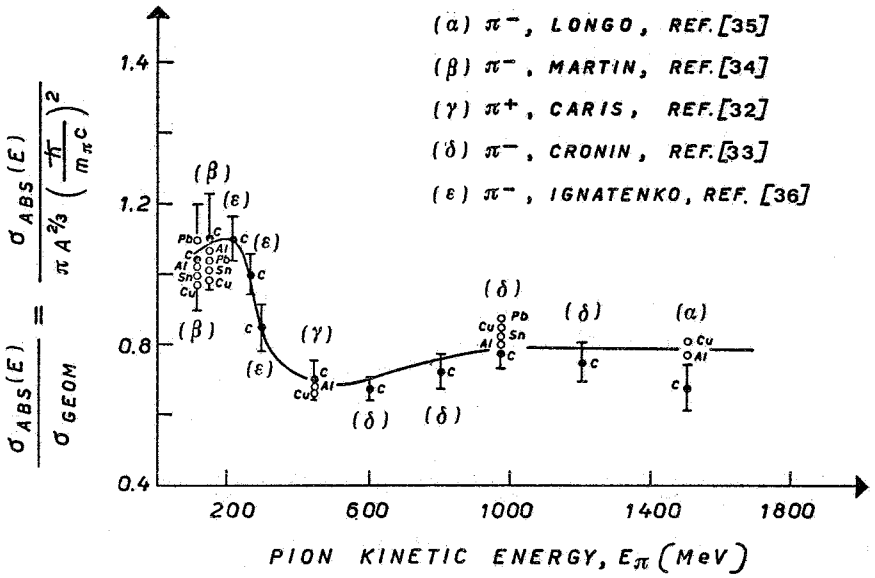

FIG. B.1. - Ratio $R(E_\pi) = \sigma_{abs} / \sigma_{geom}$ of the absorption cross-section over the geometrical cross-section as a function of the pion kinetic energy E_π.

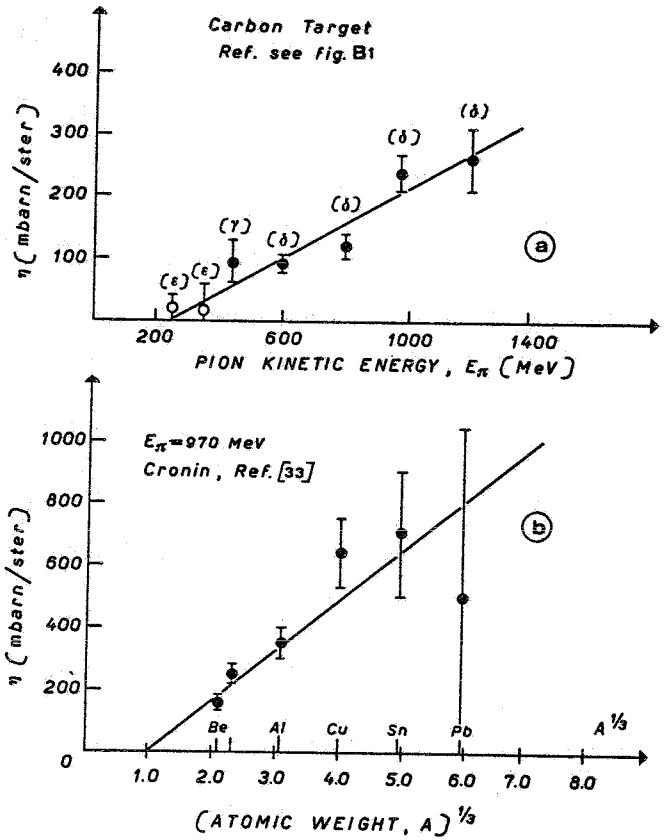

FIG. B.2. - Cross-section for secondary particle production. a) in carbon, as a function of the incident pion kinetic energy; b) as a function of the atomic weight, A, of the absorber, at $E_\pi = 970$ MeV of the incident pion kinetic energy.

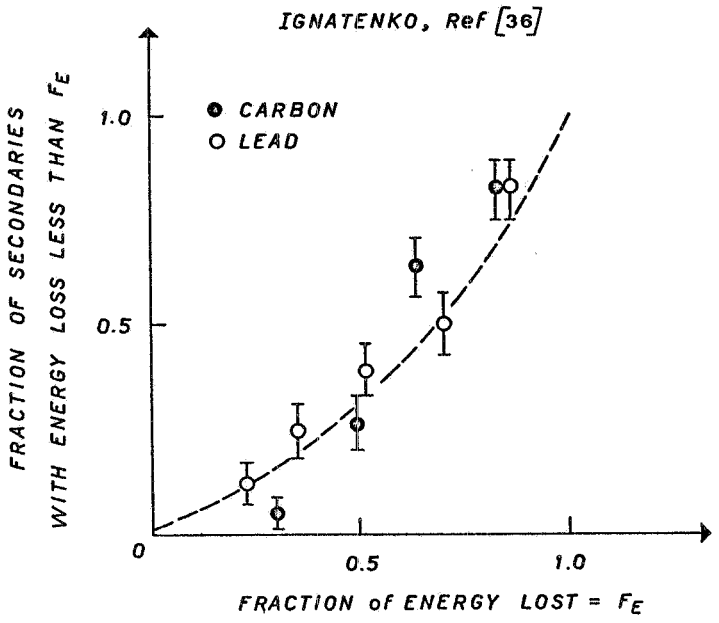

FIG. B.3 - Fraction of secondaries with an energy loss less than F_E.

Since, by definition, $\sigma_{geom} R(E_\pi) = \sigma_{abs}$, that is

$$\lambda_{geom} = \frac{A}{\sigma_{geom} \mathcal{N}_A} = \frac{A}{\sigma_{abs} \mathcal{N}_A} R(E_\pi) = \lambda_{abs} R(E_\pi);$$

we can rewrite Eq. (B.5) as follows:

$$N_{tot} = N_{tot,\,pr} + N_{tot,\,sec} = \left(N_o\, e^{-\sum_{i=1}^{n} \frac{x_i}{\lambda_{i,\,geom}} R(E_\pi)}\right) F_C \qquad \text{(B.8)}$$

with

$$F_C = 1 + \sum_{i=1}^{n} \frac{x_i\, \sigma_{i,\,sec} \mathcal{N}_A}{A}$$

Notice that F_C is a correction factor multiplying the normal absorption term (B.1) $N_{tot,\,pr}$.

B.4. - Calculation of corrections. -

From the list of materials given in Table B.I we can first calculate the absorption corrections $N_{tot,\,pr}$, i.e. the first terms of equation B.8. This calculation gives for each of the counters we are interested in (i.e. trigger counters = $AB(C+D)$; "mark" counters = $AB(C+D)(CR_1+CR_2)$; anticoincidence counters = $= AB(C+D)(\overline{CR_3+CR_4})$):

$$N_{pr,Trigger} = (N_o e^{-\sum_{i=1}^{n} \frac{x_i}{\lambda_{i,geom}} R(E_\pi)}) = N_o e^{-0.27\, R(E_\pi)};$$

$$N_{pr,mark} = N_o e^{-2.1\, R(E_\pi)}; \qquad N_{pr,AC} = N_o e^{-2.67\, R(E_\pi)}.$$

As an example for 400 MeV pions, the fraction of remaining particles at each final counter plane is:

Trigger counters = 80%; "mark" counters = 17%; anticoincidence counters = 11%.

To evaluate the effect of secondary corrections we must, in addition, use the solid angle of each final counter as seen by each absorber and the range cut for each absorber. The values of F_C (second term in Eq. (B.8), for several incident pion energies, are listed in Table B.II.

TABLE B.II

The values of F_C (secondary particle production correction) are listed for different pion kinetic energies and for the three different final counters we are interested in.

Pion kinetic energy E_π (MeV)	F_C		
	Trigger counters	"mark" counters	anticoincidence counters
400	1.047	1.000	
500	1.099	1.098	
600	1.150	1.588	1.133
1000	1.413	5.159	3.24
1500	1.573	10.61	8.389

As can be seen from Eq. (B.8) when $F_C(E_\pi)$ is equal to $\exp(+\sum_{i=1}^{n} x_i/\lambda_{i,abs})$ all the absorbed pions have produced a secondary that reached the final counter. Clearly for energies higher than this "balanced" absorption "energy there is not a correction for pion absorption. For our apparatus this "balanced absorption" energy point is for each counter respectively:

Trigger counters $\simeq$ 800 MeV; "mark" counters $\simeq$ 1000 MeV;

anticoincidence counters $\simeq$ 1500 MeV.

All of the calculation in Table B.II refer to secondary corrections for a single track.

The effects of all these corrections on the detection efficiencies for various produced final states are discussed in Appendix A.

FOOTNOTES AND REFERENCES. -

(1) - J.E. Augustin, J.C. Bizot, J. Buon, J. Haissinski, D. Lalanne, P. Marin, J. Perez-y-Jorba, F. Rumpf, E. Silva and S. Tavernier, Phys. Rev. Letters 20, 126 (1968); J.E. Augustin, D. Benaksas, J. Buon, F. Fulda, V. Gracco, J. Haissinski, D. Lalanne, F. La Planche, J. Lefrancois, P. Lehmann, P. Marin, J. Perez-y-Jorba, F. Rumpf and E. Silva, Lett. Nuovo Cimento 2, 214 (1969); J.C. Bizot, B. Delcourt, J. Jeanjean, D. Lalanne, J. Perez-y-Jorba, F. Richard, F. Rumpf and D. Trielle, Lett. Nuovo Cimento 4, 1273 (1970).

(2) - U.L. Auslander, G.I. Budker, Ju.N. Pestov, V.A. Sidorov, A.N. Skrinsky, and A.G. Khabakhpashev, Phys. Letters 25b, 433 (1967); V.E. Balakin, G.I. Budker, E.V. Pakhtosova, V.A. Sidorov, A.N. Skrinsky, G.M. Tumaikin and A.G. Khabakhpashev, Phys. Letters 34b, 328 (1971).

(3) - Boson group: B. Bartoli, B. Coluzzi, F. Felicetti, G. Goggi, G. Marini, F. Massa, D. Scannicchio, V. Silvestrini and F. Vanoli, Nuovo Cimento 70A, 603 (1970); Nuovo Cimento 70A, 615 (1970).

(4) - Boson group: B. Bartoli, F. Felicetti, G. Marini, A. Nigro, H. Ogren, N. Spinelli, V. Silvestrini and F. Vanoli, Phys. Letters 36B, 593 (1971); Phys. Letters 36B, 598 (1971).

(5) - Frascati-Roma-Padova-Maryland Collaboration ($\mu\pi$ group): B. Borgia, M. Conversi, M. Grilli, E. Iarocci, M. Nigro, L. Paoluzi, P. Spillantini, L. Trasatti, V. Valente, R. Visentin and G.T. Zorn, Intern. Symp. on Electron and Photon Interactions at High Energies, Cornell (1971).

(6) - $\gamma\gamma$ group: C. Bacci, R. Baldini-Celio, G. Capon, C. Mencuccini, G.P. Murtas, G. Penso, A. Reale, G. Salvini, M. Spinetti and B. Stella, 1971 Intern. Symp. on Electron and Photon Interactions at High Energies, Cornell (1971).

(7) - Among others: S. Ferrara, M. Greco and A.F. Grillo, Lett. Nuovo Cimento 4, 1 (1970); N. Cabibbo, G. Parisi and M. Testa, Lett. Nuovo Cimento 4, 34 (1970); J.D. Bjorken and S.J. Brodsky, Phys. Rev. D1, 1416 (1970); G. Kramer, J.L. Uretsky and T.F. Walsh, DESY report 70/44 (1970); J. Layssac and F.M. Renard, Lett. Nuovo Cimento 1, 197 (1971); M.T. Vaughn and P.J. Polito, Lett. Nuovo Cimento 1, 74 (1971); A. Bramon and M. Greco, Lett. Nuovo Cimento 1, 739 (1971) and Frascati reports LNF-71/8 (1971), LNF-71/97 (1971); etc.

(8) - E.D. Bloom, D.H. Coward, H. De Staebler, J. Drees, G. Miller, L.W. Mo, R.E. Taylor, M. Breidenbach, J.I. Friedman, G.H. Hartmann, H.W. Kendall, Phys. Rev. Letters 23, 930 (1969); M. Breidenbach, J.I. Friedmann, H.W. Kendall, E.D. Bloom, D.H. Coward, H. De Staebler, J. Drees, L.W. Mo, R.E. Taylor, Phys. Rev. Letters, 23, 935 (1969).

(9) - The source of our events (which is defined as the region of interaction of positron and electron bunches) has a finite energy dependent length. In fact it is expected to have a longitudinal distribution

$$N(l_z) = N_o \exp(-l_z^2/2\bar{l}_z^2)$$

where $\bar{l}_z$(cm) is theoretically expected to be $20 \times E^{3/2}$ (E_+ GeV) and experimentally has been determined as $(22 \pm 2)E^{3/2}$ (private comunication of the Adone machine staff). This reduces the effective solid angle of the apparatus by a factor of the order of 2.

(10) - In each chamber, the magnetostrictive pick-up coil was placed at the edge which is nearer to the horizontal plane: i.e. at $\varphi = 28^o$ and 332^o for chambers 1 and 4, and at $\varphi = 152^o$ and 208^o for chambers 2 and 3.

(11) - In Adone there are three bunches of e^+ and three bunches of e^-, each of duration $\sim$ 1-2 nsec (f.w.h.m.). They cross the RF cavity when the phase has a

fixed value Φ (syncronous phase, slightly dependent on the machine energy), and collide in the experimental sections every ~117 nsec. The beam-beam impact occurs thus at a fixed time with respect to the time when the RF phase assumes its synchronous value Φ.

(12) - We recall that the luminosity L of a storage ring at one of the interaction regions for head-on-collisions of two beams uniformly distributed into k bunches per beam, with over lapping transverse gaussian distributions whose r.m.s. dimensions $\bar{l}_x$, $\bar{l}_y$ are equal, is given by

$$L = \frac{1}{k f_o e^2} \frac{I_{e^+} I_{e^-}}{4\pi \bar{l}_x \bar{l}_y}$$

where I_{e^+} and I_{e^-} are the positron and electron beam currents, f_o is the revolution frequency of the beams, and e is the electronic charge. L provides a measurement of the machine intensity, in the sense that the rate $\dot{n}$ of events produced at one crossing region from a process of cross-section σ is given by $\dot{n} = L\sigma$.

(13) - G. Barbiellini, B. Borgia, M. Conversi and R. Santonico, Rendiconti della Classe di Scienze Mat., Fis. e Nat. dell'Accad. Naz. dei Lincei 44, 233 (1968); H.C. Dehne and M. Preger, Frascati report LNF-70/33 (1970).

(14) - It is worthwile to note that an independent check of luminosity performed by the machine group measuring the γ rays emitted at forward angles from e^+e^- single and double bremsstrahlung reactions, agrees, to within ~10%, with the Bhabha "monitor" luminosity data.

(15) - By definition, $\Delta\varphi$ is zero when the two particles go in opposite directions. Particularly for the multiparticle analysis, we have found it convenient to define the sign of $\Delta\varphi$ in a specular way for left and right telescopes. I.e. if we consider the two half planes defined by the azimuthal projection of the particle trajectory which goes in a top telescope, (T_1 or T_2), $\Delta\varphi$ will be positive if the second particle lies in the half plane containing the other top telescope. (In the multiparticle case, if both particles go in the bottom telescopes $\Delta\varphi$ is consistently defined as positive).

(16) - The inefficiencies of our monogap spark chambers, which are essentially due to impurity in the Ne-He gas and malfunctioning of the trigger spark gaps, are variable in time and differ for the various chambers. The values, averaged on the whole period, turned out to be: $\varepsilon_{\alpha_1} = 0.86$, $\varepsilon_{\beta_1} = 0.71$, $\varepsilon_{\alpha_2} = 0.86$, $\varepsilon_{\beta_2} = 0.85$, $\varepsilon_{\alpha_3} = 0.85$, $\varepsilon_{\beta_3} = 0.84$, $\varepsilon_{\alpha_4} = 0.89$, $\varepsilon_{\beta_4} = 0.93$. They have been experimentally determined from the analysis of the e^+e^- scattering events in which only one chamber had not fired.

(17) - Y.S. Tsai, Intern. Simp. on High Energy Electron and Photon Interactions at High Energy, Hamburg (1965), pag. 380 and Phys. Rev. 120, 269 (1960); V.N. Bayer and S.A. Kheifets, Nuclear Phys. 47, 313 (1963).

(18) - S. Tavernier, Thesis, Orsay Intern. Report 68/7 (1968).

(19) - A. Rich, Phys. Rev. Letters 20, 967 (1968).

(19 bis) - As was described in Section III, the monitor apparatus is operated in a contiguous straight section of Adone. Due to the symmetry of the machine and the fact that the data were collected during a long period of time (averaging over

slight variations in the working conditions), it is reasonable to assume that the overall results are unaffected by the fact that small and large angle elastic scattering were measured in different straight sections of Adone.

(20) - M. Curatolo, University of Rome Thesis, unpublished.

(20 bis) - If one wants to express the experimental result in terms of a cut-off parameter Λ, using an amplitude modification $(1 \pm q^2/\Lambda_{\pm}^2)^{-1}$, from the quoted errors one obtains (at a 95% confidence level)

$$\Lambda_+ = 3.9 \text{ GeV/c} \qquad \Lambda_- = 5.4 \text{ GeV/c}$$

The q^2 value used ($q^2 = 1.52$ (GeV/c)^2) corresponds to the center of the energy range explored.

(21) - For example: two particles entering the two top (bottom) telescopes T_1, T_2 (T_3, T_4) will have, by definition, positive $\Delta\varphi$, while the $\Delta\varphi$ corresponding to particles entering vertical pair of telescopes (T_1, T_4 or T_2, T_3) will have negative sign.

(22) - V.N. Baier and V.S. Fadin, Phys. Letters 53 B, 156 (1971).

(23) - The theoretical $\Delta\varphi$ distribution for the $e^+e^- \rightarrow e^+e^-\pi^+\pi^-$ reaction in quite similar to the distribution for $e^+e^- \rightarrow e^+e^- e^+e^-$ shown in Fig. 15(a). See S.J. Brodsky, J. Kinoshita and H. Terazawa, Phys. Rev. 4D, 1532 (1971).

(24) - The M.C. program is the same we have used to compute the detection efficiency of non-coplanar events. The electrons were generated according to the QED scattering cross section. Spark chamber efficiencies and effects of the extended source (see Ref. (9), Section II) were taken into account, as well as all the geometrical features of the apparatus (cfr. also Appendix A).

(25) - The spark efficiency of the monogap spark chambers depends among the other on the angle ψ between the direction of the particle which cross the chamber and the normal to the chamber plates. Due to the finite longitudinal dimension of the source which is comparable to the linear dimensions of our apparatus (see Ref. (9), Section II), the ψ distribution of the particles associated with non-coplanar events is broader than the corresponding Bhabha electrons ψ distribution. Consequently the non-coplanar particles are detected by our spark chambers with efficiencies $\varepsilon_{n.c.}$ which are lower than the spark efficiencies for Bhabha electrons ε_e (listed in Ref. (9)), by a factor which has been experimentally determined to be $\gamma = \varepsilon_{n.c.} / \varepsilon_e = 0.95 \pm 0.01$.

(26) - A. Bramon and M.T. Greco, Frascati Report LNF-71/97 (1971); M.T. Vaughn and P.J. Polito, Lett. Nuovo Cimento, 1, 74 (1971); J. Layssac and F.M. Renard, Lett. Nuovo Cimento 1, 197 (1971); Montpellier Preprint PM/71/2 (1971).

(27) - M. Davier, I. Derado, D.C. Fries, F.F. Liu, R.Z. Mozley, A.C. Odian, J. Park, W.P. Swanson, F. Villa and D. Yount SLAC preprint, June 30 (1971).

(28) - However, the situation is quantitatively different at different energies. While at 1.82 and 2.3 GeV C.M. energies the acceptable solutions turn out to have a $P(\chi^2) \geq 65\%$, at 1.51 GeV no solution was found with $P(\chi^2) > 10\%$. This is due to the fact that the fraction of "marked" events at 1.51 GeV is experimentally $(15 \pm 5)\%$, which is about two standard deviations above the predictions of any possible fit. This difference contributes ~ 4 to the χ^2 of all solutions. After having tested that a one standard deviation downwards shift of f_M (at 1.51 GeV) would reproduce the same χ^2 distributions we found at the other energies, and that the cross-section values would be unaffected, we have lowered, at 1.51 GeV, the $P(\chi^2)$ cut to 5%.

(29) - F. Cerulus, Suppl. Nuovo Cimento 15, 402 (1960).

(30) - For example, the experimental determination of the ratio $x = \sigma_{2\pi^\pm, N} / \sigma_{\geq 4\pi^\pm, TOT}$ by the other Adone groups can be seen directly from Figs. (23(b) and (c).

(31a) - ACO results: J. Lefrancois, Invited talk on the Orsay results at the International Symposium on Electron and Photon Interactions at High Energy, Cornell (1971).
(31b) - Novosibirsk results: V. A. Sidorov, Invited talk on the Novosibirsk results at the International Symposium on Electron and Photon Interactions at High Energy, Cornell (1971).
(31c) - Adone $\gamma\gamma$ group results: C. Bacci, R. Baldini-Celio, G. Capon, C. Mencuccini, G. P. Murtas, G. Penso, A. Reale, G. Salvini, M. Spinetti and B. Stella, Phys. Letters (to be published).
(31d) - Adone $\mu\pi$ group results: G. Barbarino, F. Ceradini, M. Conversi, M. Grilli, E. Iarocci, M. Nigro, L. Paoluzi, R. Santonico, P. Spillantini, L. Trasatti, V. Valente, R. Visentin and G. T. Zorn, Nuovo Cimento (to be published); see also M. Grilli, Lectures given at the Intern. School of Yerevan Physical Institute, Frascati report LNF-71/100 (1971).
(32) - J. C. Caris, E. A. Knapp, V. Perez-Mendez and W. A. Perkins, Phys. Rev. 126, 295 (1962).
(33) - J. W. Cronin, R. Cool and A. Abashian, Phys. Rev. 107, 1121 (1957).
(34) - R. L. Martin, Phys. Rev. 87, 1052 (1954).
(35) - M. J. Longo and B. J. Moyer, Phys. Rev. 125, 701 (1962).
(36) - A. E. Ignatenko, CERN Symposium (1956), vol. 2, p. 313.